

Surface-Stimulated Phenomena in the Polarization Response of Ferroelectrics

THÈSE N° 4082 (2008)

PRÉSENTÉE LE 30 MAI 2008

À LA FACULTÉ DES SCIENCES ET TECHNIQUES DE L'INGÉNIEUR
LABORATOIRE DE CÉRAMIQUE
PROGRAMME DOCTORAL EN SCIENCE ET GÉNIE DES MATÉRIAUX

ÉCOLE POLYTECHNIQUE FÉDÉRALE DE LAUSANNE

POUR L'OBTENTION DU GRADE DE DOCTEUR ÈS SCIENCES

PAR

Guido GERRA

Master of Philosophy, University of Cambridge
et de nationalité italienne

acceptée sur proposition du jury:

Prof. K. Scrivener, présidente du jury
Prof. N. Setter, Dr A. Tagantsev, directeurs de thèse
Prof. J. Junquera, rapporteur
Prof. A. Pasquarello, rapporteur
Prof. J. Petzelt, rapporteur



ÉCOLE POLYTECHNIQUE
FÉDÉRALE DE LAUSANNE

Suisse
2008

Abstract

The integration of ferroelectrics in electronic devices requires that they be used in the form of thin films, which implies that for such systems finite-size effects related to the presence of a ferroelectric-electrode interface become important. In this thesis, a number of theoretical studies are presented on the properties of metal-ferroelectric-metal structures, focusing on the impact of the metal-ferroelectric interface on the polarization response of the system.

First, a model for reverse domain nucleation in ferroelectrics is introduced, which takes into account the ferroelectric-electrode coupling in both the homogeneous and random cases. The model provides a solution to the coercivity paradox—i.e., the large discrepancy between the observed and predicted coercive fields. The possibility of non-thermally activated nucleation of reverse domains is demonstrated. It is found that small inhomogeneities in the ferroelectric-electrode interface may lead to an exponentially wide spectrum of waiting times for switching. The model predicts that switching is facilitated near morphotropic phase boundaries in perovskite-type ferroelectrics.

In order to quantitatively analyze the size-effect problem in metal-ferroelectric-metal systems, an approach is developed which combines first-principles calculations and phenomenological theory. The parameters of the model can be extracted from calculations on ultrathin films, while experimentally verifiable predictions can be made on thick films.

Using the developed approach, it is demonstrated how the size effect can be separated into two distinct contributions: a long-range electrostatic and a short-range “chemical” one. By considering symmetric $\text{SrRuO}_3/\text{BaTiO}_3/\text{SrRuO}_3$ heterostructures with different types of termination ($\text{TiO}_2\text{-TiO}_2$ or $\text{RuO}_2\text{-RuO}_2$), it is shown that the balance between the long-range and the short-range contribution to the size effect can be essentially affected by the type of termination of the ferroelectric and by the polarization hardness of the electrode. The leading role of the long-range contribution to the size effect in $\text{SrRuO}_3/\text{BaTiO}_3/\text{SrRuO}_3$ heterostructures is demonstrated.

Application of the approach to the case of $\text{SrRuO}_3/\text{BaTiO}_3/\text{SrRuO}_3$ het-

erostructures with asymmetric interfaces enables to provide a quantitative description of a number of manifestations of such asymmetry in films of technologically meaningful thickness. In particular, it is found that the asymmetry exerts a poling effect on the films, leading to a smearing of the phase transition, to an induced piezoelectric response above the transition temperature, and to the reversal of the polarization asymmetry by application of biaxial strain.

Another important result of such calculations is the observation that the ionic relaxations in the metal-oxide electrode play a crucial role in stabilizing the ferroelectric phase of the films. Comparison with frozen-phonon calculations shows that the degree of softness of the SrRuO₃ lattice has an essential impact on the screening of ferroelectric polarization, reducing the critical thickness for ferroelectricity of the system. These results provide a possible explanation for the observed beneficial impact of oxide electrodes on the switching and dielectric properties of ferroelectric capacitors.

Keywords: ferroelectricity, thin films, theory, ab initio, domain nucleation, size effect, screening

Resumé

L'intégration des matériaux ferroélectriques dans des dispositifs électroniques exige qu'ils soient employés sous forme de couches minces, ce qui implique que pour de tels systèmes des effets de taille finie, reliés à la présence d'une interface entre le ferroélectrique et l'électrode, deviennent importants. Dans ce travail de thèse, on présente un certain nombre d'études théoriques sur les propriétés des structures métal-ferroélectrique-métal, se concentrant sur l'impact de l'interface entre le métal et le ferroélectrique sur la réponse de polarisation du système.

D'abord, on présente un modèle pour la nucléation de domaines inversés dans le ferroélectrique, qui tient compte du couplage entre le ferroélectrique et l'électrode, dans les cas homogène et aléatoire. Le modèle fournit une solution au paradoxe de la coercivité, c.à.d. la grande différence entre les champs coercitifs observés et prévus. On démontre la possibilité de la nucléation non thermiquement activée des domaines inversés. On constate que des petites inhomogénéités dans l'interface ferroélectrique-électrode peuvent mener à une gamme exponentiellement étendue de temps d'attente pour le basculement de la polarisation. Le modèle prévoit que le basculement est facilité près des frontières de phase morphotropique dans les ferroélectriques de la famille des pérovskites.

Afin d'analyser quantitativement le problème de l'effet de taille finie dans des systèmes métal-ferroélectrique-métal, on développe une approche qui combine des calculs « ab-initio » et la théorie phénoménologique. Les paramètres du modèle peuvent être extraits à partir de calculs sur des couches ultra-minces, alors que des prévisions expérimentalement vérifiables peuvent être faites sur des films épais.

En utilisant l'approche développée, on démontre comment l'effet de taille finie peut être séparé dans deux contributions distinctes : une électrostatique à longue portée et une chimique à courte portée. En considérant des hétérostructures symétriques de $\text{SrRuO}_3/\text{BaTiO}_3/\text{SrRuO}_3$ avec différents types de terminaison ($\text{TiO}_2\text{-TiO}_2$ ou $\text{RuO}_2\text{-RuO}_2$), on montre que l'équilibre entre la contribution à longue portée et à courte portée peut être essentielle-

ment affecté par le type de terminaison du ferroélectrique et par la « dureté » de polarisation de l'électrode. On démontre le rôle prépondérant de la contribution à longue portée à l'effet de taille finie dans des hétérostructures de $\text{SrRuO}_3/\text{BaTiO}_3/\text{SrRuO}_3$.

L'application de l'approche au cas d'hétérostructures de $\text{SrRuO}_3/\text{BaTiO}_3/\text{SrRuO}_3$ avec interfaces asymétriques, nous permet de fournir une description quantitative d'un certain nombre de manifestations d'une telle asymétrie, en films d'épaisseur technologiquement importante. En particulier, on constate que l'asymétrie exerce un effet polarisant sur les films, menant à un élargissement de la transition de phase, à une réponse piézoélectrique induite au-dessus de la température de transition, et à l'inversion de l'asymétrie de polarisation par application d'une contrainte biaxiale.

Un autre résultat important de nos calculs est l'observation que les relaxations ioniques dans l'électrode d'oxyde métallique jouent un rôle crucial en stabilisant la phase ferroélectrique des films. La comparaison avec des calculs de type « frozen-phonon » prouve que le degré de « mollesse » du réseau cristallin de SrRuO_3 a un impact essentiel sur l'écrantage de la polarisation ferroélectrique, réduisant l'épaisseur critique pour la ferroélectricité du système. Ces résultats fournissent une explication possible pour l'impact favorable, observé expérimentalement, des électrodes d'oxyde sur les propriétés diélectriques et sur le basculement de la polarisation des condensateurs ferroélectriques.

Mots-clés: ferroélectricité, couches minces, théorie, ab initio, nucléation de domaines, effet de taille finie, écrantage

Acknowledgements

A doctoral thesis, like an epic journey into the unknown, may lead its author astray and leave him groping in dismay without the watchful eye of a Virgil. Well, *my* Virgil was Prof. Alexander Tagantsev. His grasp of physics, his deep and vast knowledge of ferroelectricity, but most of all his vision and ability to discern priorities have guided me successfully across the troubled waters of doctoral work and then safely to shore.

My thesis director, Prof. Nava Setter, who trusted me—back in 2003 and throughout my time at EPFL—as a worthy candidate for a doctorate and without whose support—both practical and moral—this thesis would not have been, will have my gratitude evermore.

I then wish to express my gratitude to the entire personnel of the Ceramics Laboratory, from both a professional and personal point of view. A number of colleagues deserve a special mention, for all their scientific and technical—as well as moral—support: Dr. Vladimir Sherman, Dr. Tomoaki Yamada, Dr. Yongli Wang, Dr. Roman Gysel, Dr. Matthew Davis, Dr. Marko Budimir, Dr. Kyle Brinkman, Dr. Viktor Porokhonsky, Dr. Igor Stolichnov, Dr. Pavel Mokřý, Mr. Andreas Nöth, Mr. Lino Olivetta, Mr. Jacques Castano; and all the others—especially Ms. Naama Klein, Mr. Sebastian Riester and Dr. Scott Harada—for their personal support and friendship. Many thanks to Prof. Dragan Damjanovic and Prof. Paul Muralt for their useful comments at lab seminars, and to Ms. Eva Favre and Ms. Yuko Kagata Spitteler for their administrative support.

I would like to thank Prof. Krzysztof Parlinski of the Institute of Nuclear Physics, Polish Academy of Sciences in Krakow, for introducing me to the use of VASP and for the many fruitful discussions. I would also like to thank the members of my thesis jury: Dr. Javier Junquera, Prof. Alfredo Pasquarello, Prof. Jan Petzelt and Prof. Karen Scrivener.

Finally, I would like to thank my family, all my friends around the world and of course Claudia. Your love and support provided me with that precious peace of mind which is an essential ingredient to the completion of such an intellectual task.

Contents

1	Introduction	1
1.1	A Few Definitions	2
1.1.1	Ferroelectric, pyroelectric, and piezoelectric materials	2
1.1.2	The Curie-Weiss law	2
1.1.3	Perovskite ferroelectrics and barium titanate	3
1.1.4	Electrostriction	4
1.1.5	Ferroelectric domains and hysteresis	5
1.1.6	Industrial applications of ferroelectrics	6
1.2	Landau Theory	7
1.2.1	Second order phase transitions	8
1.2.2	First order phase transitions	9
1.3	First-Principles Calculations	10
2	State of the Art	15
2.1	Domain nucleation in ferroelectrics	15
2.2	Interface-related phenomena	19
2.3	Critical thickness for ferroelectricity	24
3	Surface-Stimulated Domain Nucleation in Ferroelectrics	29
4	Combined First-Principles–Phenomenological Approach	39
4.1	Framework	40
4.2	Applicability	44
5	Short- and Long-Range Contributions to the Size Effect	47
5.1	Calculations	49
5.2	Results	52
6	Asymmetric Ferroelectric-Electrode Interfaces	57
6.1	The free energy of asymmetric heterostructures	57
6.2	Results	61

7 In-Situ Polarization Screening	65
8 Conclusions and Perspectives	73
Bibliography	77
Publications and Conferences	83
Curriculum Vitae	85

*“Considerate la vostra semenza:
fatti non foste a viver come bruti,
ma per seguir virtute e canoscenza”*

(Consider your sowing:
you were not made to live like brutes,
but to follow virtue and knowledge)

Dante Alighieri, *Inferno*, Canto XXVI, 118-120

Chapter 1

Introduction

The history of ferroelectricity began in 1920 when Joseph Valasek discerned electric hysteresis in the dielectric response of Rochelle salt [1,2]. Some 90 years later, while the employment of ferroelectrics in bulk commercial devices is widespread, their application within the microelectronics industry is still quite limited. One of the main problems that curb the integration of ferroelectric memories in electronic circuitry and computers is that when the size of the single component approaches the nanoscale, the behavior of the ferroelectric deviates from that of the bulk, often degrading its performance. In the case of thin films, the main difference is of course the presence of a surface or an interface with a second material and the fact that the surface-to-volume ratio is much larger than in the bulk. The termination of the crystal has a number of important consequences. First, the finite spontaneous ferroelectric polarization at the surface implies a finite space charge, which is very expensive in terms of electrostatic energy and therefore must be somehow screened. Second, the inversion symmetry of the normal component of the polarization is broken, and there thus appears a preferable polarization direction—in other words, the surface exerts a poling effect on the film. Moreover, the symmetry breaking introduces a two-dimensional critical system, whose order parameter, the surface polarization, requires energy to be sustained. Third, we must consider the mechanical boundary conditions of the system, which have a significant impact on the properties of the ferroelectric. Finally, whenever the film surface is in contact with a second crystal or a fluid, short-range electronic interactions between the different atomic species bring about a change in the chemical environment and thus in the local structure of the lattice. All these phenomena affect the polarization response of the film and must be fully understood in order to control the behavior of ferroelectric thin-film devices.

This thesis is devoted mostly to these four issues. In the following sec-

tions, we will introduce the fundamental concepts lying behind the physics of ferroelectrics and the theoretical tools available nowadays to tackle problems in ferroelectricity. In Chapter 2, the state of the art in the field of interest of this thesis will be reviewed, with particular emphasis laid upon the problem of domain nucleation, of passive layers, and of the critical thickness for ferroelectricity. A solution to the first of these problems, the Landauer paradox, or the apparent contradiction between the theory of domain nucleation and experimental observations, will be discussed in Chapter 3. Chapter 4 introduces a combined first-principles–phenomenological approach to studying the interface properties of ferroelectric-electrode thin-film heterostructures, an approach which is then used in Chapters 5 and 6 to describe the interface between a BaTiO_3 and a SrRuO_3 plate. An important result of these studies is discussed in Chapter 7: the relative softness of the oxide-electrode lattice with respect to ionic polarization and the impact of such a phenomenon on the critical thickness for ferroelectricity of the system. Finally, the conclusions will be drawn in Chapter 8.

1.1 A Few Definitions

1.1.1 Ferroelectric, pyroelectric, and piezoelectric materials

We call *ferroelectric* a material possessing an electric polarization which is stable in the absence of external electric fields and whose direction can be reversed by the application of an electric field. Since ferroelectricity implies polarity in a crystal, ferroelectric materials must belong to one of the ten polar point groups. It follows that a ferroelectric crystal is also *pyroelectric*—i.e., a change in the temperature of the crystal results in a change of the value of its polarization due to thermal expansion. Moreover, as a polar crystal is non-centrosymmetric, the application of mechanical stress induces a variation in the value of its polarization. Conversely, the application of an electric field results in a mechanical deformation of the crystal proportional to the applied field. In other words, a ferroelectric crystal is *piezoelectric*.

1.1.2 The Curie-Weiss law

The polar symmetry of a ferroelectric crystal can always be related to a higher-symmetry structure, known as the *prototype* phase, from which it is obtained by small structural perturbations. For most materials, such prototype phase is non-polar and stable at high temperatures. At a certain critical

temperature, known as the *Curie temperature*, T_c , the crystal undergoes a phase transition from the *paraelectric* prototype phase to the *ferroelectric* phase, accompanied by the appearance of a spontaneous polarization. The onset of polarization can either be a continuous function of temperature—in which case we speak of a *second-order* phase transition—or a discontinuous one—in which case we speak of a *first-order* phase transition. The difference between a first- and a second-order phase transition is most notably seen in the behavior of the dielectric susceptibility, χ , at T_c . According to the Curie-Weiss law, the susceptibility above the Curie temperature behaves as $\chi = C/(T - T_0)$, where T_0 is the Curie-Weiss temperature and C the Curie-Weiss constant. In the case of second-order phase transitions, $T_c = T_0$ and the susceptibility has a singularity at the transition temperature, while in the case of first-order transitions, $T_c > T_0$ and χ remains finite at T_c . A more detailed account of ferroelectric phase transitions will be given in Section 1.2.

From a microscopic point of view, ferroelectricity is due to the relative displacement of the cations and anions in the crystal. Ferroelectricity can thus be described by a long-wavelength (i.e., Brillouin-zone center), low-frequency transverse optic phonon mode¹, known as the *soft* mode, whose frequency is a monotonically increasing function of temperature: $\omega_s^2 \sim (T - T_0)$. On approaching the Curie-Weiss temperature T_0 , the soft-mode frequency tends to zero, and so does the force constant associated to it (hence the term *soft*). Below the Curie temperature T_c , the non-polar prototype ionic structure is deformed into a polar one.

1.1.3 Perovskite ferroelectrics and barium titanate

A large number of ferroelectric crystals possess the *perovskite* structure. A typical example of this family of crystals is BaTiO_3 . The prototype phase of BaTiO_3 has a simple-cubic Bravais lattice, with a barium ion occupying each corner of the cube, a titanium ion at the body center, and an oxygen ion at each face center [cf. Figure 1.1]. Such a structure falls into the point group $m\bar{3}m$. Below the Curie temperature, the titanium and barium ions are displaced in one direction along one of the crystallographic axes, while the three oxygen ions are displaced in the opposite direction. The new symmetry of the crystal is $4mm$. The oxygen octahedron surrounding the titanium ion [cf. Figure 1.1] gets slightly distorted, with the *apical* oxygen ion—i.e., the

¹The representation of ferroelectricity as a soft optic phonon mode is meaningful only in the case of *displacive* phase transitions. For so-called *order-disorder* ferroelectrics, the transition is not associated to a phonon mode, but rather to a change in the statistical average of a thermal hopping motion between different potential wells, each representing a polar state.

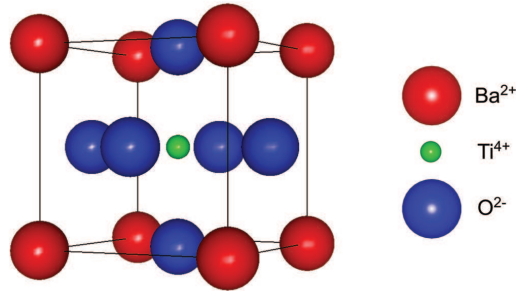


Figure 1.1: The perovskite structure of barium titanate in the prototype cubic phase. The oxygen ions, which form an octahedron surrounding the titanium ion, are equivalent by symmetry in the cubic phase, while in the tetragonal ferroelectric phase we can distinguish between the *apical* oxygens—i.e., those in the same plane as the barium ions and usually labeled O_{I} —and the *equatorial* oxygens—i.e., those in the same plane as the titanium ion and usually labeled O_{II} .

one lying in the same plane as the barium ion and usually labeled O_{I} —being displaced by a larger distance than the *equatorial* ions—i.e., those in the same plane as the titanium ion and usually labeled O_{II} . If we denote by δ_{α} the displacement of the ionic species α along the polar axis and relative to the barium ion, at room temperature we will have: $\delta_{O_{\text{I}}} \approx -0.1 \text{ \AA}$, $\delta_{O_{\text{II}}} \approx -0.06 \text{ \AA}$, and $\delta_{\text{Ti}} \approx 0.05 \text{ \AA}$ [3].

Concomitant to the appearance of polar ionic displacements inside the unit cell is a change of the Bravais lattice of BaTiO_3 from cubic to tetragonal. The lattice expands along the polar axis and contracts in the perpendicular directions, although the tetragonality ratio is quite small ($c/a \sim 1.01$ at room temperature, where c is the lattice constant along the polar axis and a the lattice constant along the other two crystallographic directions).

The cubic-to-tetragonal phase transition in BaTiO_3 occurs at 120° C . At 5° C BaTiO_3 undergoes a second phase transition from tetragonal to orthorhombic (point group mm), and at -90° C a third one from orthorhombic to rhombohedral (point group $3m$). All three transitions are of the first order.

1.1.4 Electrostriction

A fundamental phenomenon that must be considered when describing the properties of ferroelectrics is *electrostriction*, which is defined as the coupling between mechanical stress and the square of polarization. It is a property of all dielectric materials, not just of ferroelectrics, and it differs from the piezoelectric effect, which is linear in both the polarization and stress.

In ferroelectric materials, the electrostrictive effect is usually expressed in

terms of the polarization vector, P_i . The strain u_{ij} induced in a mechanically free dielectric by electrostriction can be written as:

$$u_{ij} = Q_{ijkl}P_kP_l, \quad (1.1)$$

where Q_{ijkl} is the fourth-rank tensor describing electrostriction in anisotropic media. If the material is mechanically clamped, the electrostrictive effect is described by a relation between the polarization and the mechanical stress σ_{ij} induced in the material:

$$\sigma_{ij} = q_{ijkl}P_kP_l. \quad (1.2)$$

The two electrostrictive tensors, Q_{ijkl} and q_{ijkl} , are related by the following expression:

$$q_{ijmn} = c_{ijkl}Q_{klmn}, \quad (1.3)$$

where c_{ijkl} is the elastic tensor.

1.1.5 Ferroelectric domains and hysteresis

If we take a close look at a ferroelectric crystal below the Curie temperature and in the absence of electric fields, we will observe a complicated pattern of ferroelectric *domains*—i.e., regions of uniform polarization, each with a polarization vector oriented along one of the polar axes of the crystal. When an electric field is applied to the material, some domains realign so as to maximize the macroscopic polarization component parallel to the field, with the effect of minimizing the electrostatic energy. The realignment actually occurs by the displacement of the domain boundaries (known as domain *walls*), so that those domains that are oriented along the field grow, and the others shrink. The domain wall motion implies the dissipation of free energy via lattice distortions, and it is therefore a thermodynamically irreversible process with an associated activation barrier. Such activation barrier is a function of the applied electric field, but can of course be overcome through thermal fluctuations as well. If the applied field is not too large, domains polarized against it can continue to exist; however, such domains become thermodynamically unstable when the field exceeds some critical value, and the crystal is then globally polarized in one direction. The alignment of the ferroelectric domains under application of an external electric field is a typical example of *hysteretic* behavior [cf. Figure 1.2].

For small applied fields, the driving force is not large enough to displace the domain walls or nucleate new domains, and the ferroelectric behaves simply as a nonlinear dielectric. At higher fields, new domains nucleate and

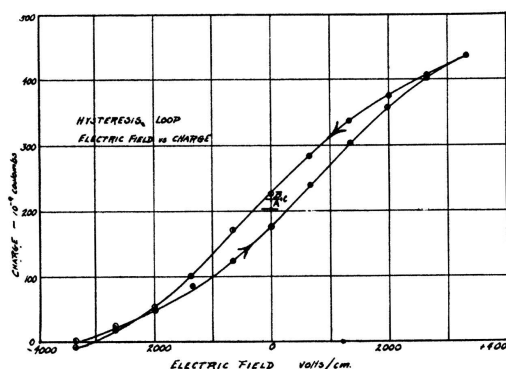


Figure 1.2: The first ferroelectric hysteresis loop to have ever appeared in the literature, measured by Valasek on Rochelle salt at room temperature [2]. The data points represent the charge at the surface (i.e., the polarization multiplied by the surface area) as a function of the applied field.

the existing domain walls move, until most of the volume of the crystal is polarized in the direction of the field, after which the polarization is said to be saturated. If we then remove the field, the crystal will retain a large macroscopic polarization referred to as *spontaneous*.

Reversal of the direction of the applied field will produce new reverse domains and enlarge the existing ones, decreasing the macroscopic value of polarization, until at what is called the *coercive* field, the polarization goes through zero and reverses its sign. The result is a *hysteresis loop*, such as the one depicted in Figure 1.2.

1.1.6 Industrial applications of ferroelectrics

The coupling between the mechanical and electrical and between the thermal and electrical response of a ferroelectric crystal has led to a broad range of industrial applications of such materials as transducers. Their pyroelectric character is utilized in thermal detectors, while their piezoelectric properties have found extensive usage in, among many others, acoustic detectors, pressure sensors, actuators, and time-measuring devices. Several other families of ferroelectric-based commercial devices stem from the electrical properties of ferroelectrics. The binary state of the ferroelectric polarization along a given crystallographic axis is exploited to make non-volatile ferroelectric random access memories (FeRAM). The extremely high values of their permittivity results in their implementation as supercapacitors. Last but not least, the nonlinearity of their dielectric response, and thus their dielectric tunability, has led to intense research recently in the telecommunications industry to

employ ferroelectrics as varactors for microwave phase shifters and for tunable frequency filters.

1.2 Landau Theory

The description of the properties of ferroelectric materials can be carried out from the macroscopic point of view of phenomenological theory, treating the material as a continuum and applying the laws of thermodynamics, elasticity theory and electromagnetism. Such description relies on the evaluation of the relevant thermodynamic potential of the system as a function of three independent variables, the state functions: temperature (T) or entropy (S) for the thermal properties, stress (σ_{ij}) or strain (u_{ij}) for the elastic properties, and electric field (E_i) or polarization (P_i) for the dielectric properties. In the present context, it is convenient to work with the following thermodynamic potential (often referred to as the electric Helmholtz free energy of the system):

$$F = U - TS - \frac{1}{2}\varepsilon_0 E^2, \quad (1.4)$$

which in differential form reads:

$$dF = -SdT + \sigma_{ij}du_{ij} + E_idP_i. \quad (1.5)$$

To describe the behavior of critical systems near the phase transition, Landau developed a phenomenological theory in which the phase transition is described by a physical quantity known as the order parameter. In the case of a ferroelectric transition, we can use as the order parameter the polarization vector. The properties of the critical system can be treated mathematically by performing a Maclaurin expansion of the relevant thermodynamic potential in terms of the order parameter. Conceptually, this corresponds to considering small deviations from the prototype phase, where we assume that $P_i = 0$ and $u_{ij} = 0$. In the most general case:

$$F = F_0 + a_{ij}P_iP_j + a_{ijkl}P_iP_jP_kP_l + a_{ijklmn}P_iP_jP_kP_lP_mP_n + \dots \\ + \frac{1}{2}c_{ijkl}u_{ij}u_{kl} - \frac{1}{2}q_{ijkl}u_{ij}P_kP_l, \quad (1.6)$$

where F_0 is the electric Helmholtz free energy of the prototype phase and where we have included explicitly the strain-polarization coupling, or electrostriction, introduced in Subsection 1.1.4. Only even powers of the polarization are present in the series, as required by symmetry in the case of a centrosymmetric paraelectric phase. The application of the Landau theory to the case of ferroelectrics is due to Devonshire [4].

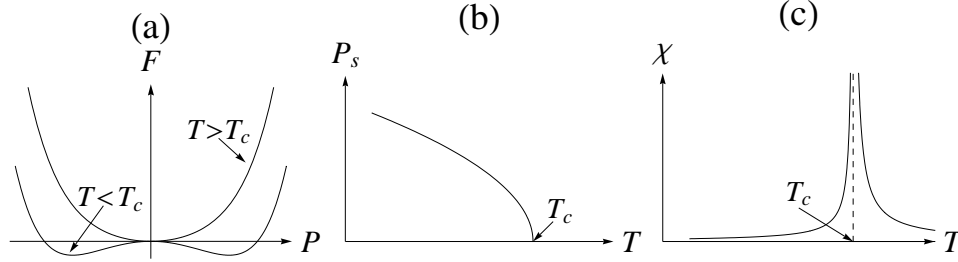


Figure 1.3: The second order phase transition: (a) shape of the electric Helmholtz free energy as a function of polarization, above and below the Curie temperature T_c ; (b) the temperature dependence of polarization; (c) the temperature dependence of the dielectric susceptibility.

In order to understand the nature of the phase transition, let us consider the simplest case, that of a uniaxial ferroelectric² under mechanically clamped ($u_{ij} = 0$) and short-circuit ($E_i = 0$) boundary conditions. The thermodynamic potential can then be written as:

$$F = F_0 + \frac{\alpha}{2}P^2 + \frac{\beta}{4}P^4 + \frac{\gamma}{6}P^6 + \dots, \quad (1.7)$$

where the coefficient α is assumed to be temperature-dependent. In particular, to reproduce the Curie-Weiss law, we must have:

$$\alpha = \frac{T - T_0}{\varepsilon_0 C}, \quad (1.8)$$

where T_0 and C are the Curie-Weiss temperature and constant defined in Subsection 1.1.2.

1.2.1 Second order phase transitions

When the Landau coefficient $\beta > 0$ (and also $\gamma > 0$), the phase transition is said to be of the second order. For temperatures greater than the Curie-Weiss temperature T_0 , the free energy has only one stationary point, the global minimum $P = 0$, and the ferroelectric crystal is in a paraelectric state [cf. Figure 1.3(a)]. Below T_0 , the state $P = 0$ becomes a local maximum, while there appear two degenerate stable states with polarization $P \neq 0$. At exactly T_0 , the three stationary points coincide, so that the transition from the zero-polarization to the finite-polarization state is smooth [cf. Figure

²A ferroelectric is said to be *uniaxial* when the order parameter has only one component, e.g. $\mathbf{P} = (P, 0, 0)$.

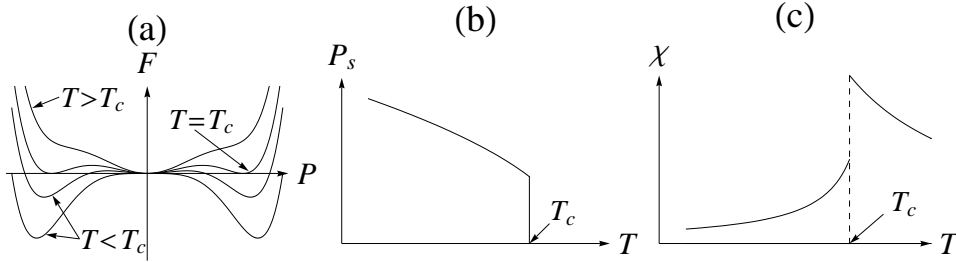


Figure 1.4: The first order phase transition: (a) shape of the electric Helmholtz free energy as a function of polarization, above and below the Curie temperature T_c ; (b) the temperature dependence of polarization; (c) the temperature dependence of the dielectric susceptibility.

1.3(b)]. In this case, the phase transition occurs at T_0 , so that $T_c = T_0$, i.e., the Curie temperature and the Curie-Weiss temperature coincide.

The spontaneous value of the polarization, P_s , is obtained by solving the equation $\partial F/\partial P = 0$, in the absence of external fields. Since P_s is a small quantity on the atomic scale³, in the free energy expansion (1.7) we can safely neglect powers of P_s greater than fourth. We can thus write:

$$P_s^2 = \frac{-\alpha}{\beta}. \quad (1.9)$$

The dielectric susceptibility is defined as: $\chi = (\partial^2 G/\partial P^2)^{-1} = (\alpha + 3\beta P^2)^{-1}$. Since $P_s = 0$ above T_c and $P_s = \sqrt{-\alpha/\beta}$ below it, we have:

$$\chi = \begin{cases} \frac{\varepsilon_0 C}{T - T_c} & \text{if } T > T_c \\ \frac{\varepsilon_0 C}{2(T_c - T)} & \text{if } T < T_c \end{cases}. \quad (1.10)$$

The susceptibility therefore diverges at T_c [cf. Figure 1.3(c)].

1.2.2 First order phase transitions

When the Landau coefficient $\beta < 0$ and $\gamma > 0$, the phase transition is said to be of the first order. In this case, the sign of β implies the possible coexistence

³From a microscopic point of view, the magnitude of the polarization can be written as $P_s = eZ_s v/\Omega$, where e is the electronic charge, Z_s the Born effective charge associated with the ferroelectric soft mode, and v is the amplitude of the soft-mode displacement vector. An atomic estimate of the polarization would involve considering a dipole with the same effective charge but with a displacement of the order of the interatomic distance $a/2$: $P_{\text{at}} = eZ_s a/2\Omega$. We therefore have: $P_s/P_{\text{at}} = 2v/a$. Since v is typically a fraction of an angstrom, it follows that $P_s \ll P_{\text{at}}$.

of two nonzero stationary polarization states [cf. Figure 1.4(a)]. These two states become local (metastable) minima well above the Curie-Weiss temperature T_0 . At a temperature $T_c > T_0$, the free energy of the two nonzero stationary states is equal to the free energy of the zero polarization state: this is where the transition between the paraelectric and ferroelectric phase occurs. We see then that unlike the case of second order phase transitions, for first order transitions the Curie temperature does not coincide with the Curie-Weiss temperature. The two are related by the following expression:

$$T_c = T_0 + C \frac{3\varepsilon_0\beta^2}{16\gamma}. \quad (1.11)$$

At T_c , the value of the spontaneous polarization on the ferroelectric side of the transition is finite [cf. Figure 1.4(b)]:

$$P_s^2 = \frac{-3\beta}{4\gamma}, \quad T = T_c. \quad (1.12)$$

As a consequence, the dielectric susceptibility $\chi = (\alpha + 3\beta P^2 + 5\gamma P^4)^{-1}$ does not diverge at T_c , but has a finite discontinuity [cf. Figure 1.4(c)]:

$$\chi = \begin{cases} \frac{16\gamma}{3\beta^2} & T \rightarrow T_c^+ \\ \frac{4\gamma}{3\beta^2} & T \rightarrow T_c^- \end{cases}. \quad (1.13)$$

1.3 First-Principles Calculations

The phenomenological Landau theory offers a very powerful tool to describe the macroscopic behavior of critical systems around the phase transition, once its set of coefficients is known. The determination of such coefficients must proceed from detailed experimental investigations. Quite often, however, information on the microscopic properties of the system is required, and it is convenient or sometimes even necessary to supplement the experimental investigations with *first-principles* calculations. In first-principles (or *ab-initio*) calculations, microscopic information is extracted from the atomic structure of the system, without need for any macroscopic input or phenomenological assumption. Nowadays, most first-principles calculations are performed within Density Functional Theory (DFT).

The starting point of DFT is the Hohenberg-Kohn theorem [5]. The theorem states that the total energy of any atomic system is a *unique functional* of the electron density, and it has its minimum value for the correct

ground-state electron density function $n(\mathbf{r})$. In other words, if we possess information about the ground-state electron distribution for given positions of the nuclei, we can derive all the ground-state properties of the system through the fundamental laws of quantum mechanics.

Let us denote by $|\Psi\rangle$ the wavefunction of an N -electron system, by $v(\mathbf{r})$ the potential due to the nuclei, and by $\hat{H} = \hat{T} + \hat{V} + \hat{U}$ the Hamiltonian, where \hat{T} , \hat{V} , and \hat{U} are the kinetic, potential, and pair-interaction energy operators, respectively. According to the Hohenberg-Kohn theorem then, the total energy of the electron system, $E_v[n] = \langle\Psi|\hat{H}|\Psi\rangle$, is a unique functional of the electron density $n(\mathbf{r})$, for a given nuclear potential $v(\mathbf{r})$. If we group together the kinetic and pair-interaction energies into a single functional $F[n] \equiv \langle\Psi|(\hat{T} + \hat{U})|\Psi\rangle$, the energy functional in atomic units⁴ takes the simple form:

$$E_v[n] = \int v(\mathbf{r})n(\mathbf{r})d\mathbf{r} + F[n]. \quad (1.14)$$

The functional $F[n]$ is universal—i.e., it is valid for any external potential and any number of electrons. Its exact analytical form is unknown, since the exact form of the many-particle wavefunction $|\Psi\rangle$ is unknown. However, by using approximations for $F[n]$, the ground state of the system can be evaluated by variational minimization of the energy with respect to the density, $\delta E_v[n]/\delta n = 0$, subject to the constraint $\int n(\mathbf{r})d\mathbf{r} = N$. It is convenient to divide $F[n]$ in three terms, the kinetic, the electron-electron Coulomb, and the exchange-correlation energies:

$$F[n] = T_s[n] + \frac{1}{2} \iint \frac{n(\mathbf{r})n(\mathbf{r}')}{|\mathbf{r} - \mathbf{r}'|} d\mathbf{r}d\mathbf{r}' + E_{xc}[n], \quad (1.15)$$

where $T_s[n] = \frac{1}{2} \int \nabla^2 n(\mathbf{r})d\mathbf{r}$ is the kinetic energy of a gas of non-interacting electrons. The simplest approximation of $F[n]$ occurs when we assume that the exchange-correlation energy can be written as

$$E_{xc}[n] = \int n(\mathbf{r})\varepsilon_{xc}(n(\mathbf{r}))d\mathbf{r}, \quad (1.16)$$

where $\varepsilon_{xc}(n(\mathbf{r}))$ is the exchange-correlation energy per electron of a homogeneous electron gas of density $n = n(\mathbf{r})$. This is called the *Local Density Approximation* (LDA). The exact analytical form of the exchange energy of a homogenous electron gas is known: $\varepsilon_x(n) = -(3/4)(3/\pi)^{1/3}n^{1/3}$ [6]. The correlation energy, $\varepsilon_c(n)$, can be calculated for a given homogeneous electron

⁴In atomic units (a.u.), the electron charge and mass and Planck's constant are all equal to unity: $e = m_e = \hbar = 1$ a.u.

density n through a Monte Carlo method [7], and its function form, $\varepsilon_c(n(\mathbf{r}))$, obtained by parameterizing the calculated $\varepsilon_c(n)$ for a number of densities [8].

If we now define the effective electrostatic potential,

$$\varphi(\mathbf{r}) \equiv v(\mathbf{r}) + \int \frac{n(\mathbf{r}')}{|\mathbf{r} - \mathbf{r}'|} d\mathbf{r}', \quad (1.17)$$

and the exchange-correlation contribution to the chemical potential of the homogeneous electron gas,

$$\mu_{xc}(n) \equiv \frac{d}{dn} [n\varepsilon_{xc}(n)], \quad (1.18)$$

variational minimization of $E_v[n]$ (subject to the constraint $\int n(\mathbf{r})d\mathbf{r} = N$) yields the following system of N one-particle Schrödinger equations:

$$\left[-\frac{1}{2}\nabla^2 + \varphi(\mathbf{r}) + \mu_{xc}(n(\mathbf{r})) \right] \phi_i(\mathbf{r}) = \varepsilon_i \phi_i(\mathbf{r}), \quad (1.19)$$

which are known as the Kohn-Sham equations [9]. The electron density is related to the Kohn-Sham orbitals ϕ_i by:

$$n(\mathbf{r}) = \sum_{i=1}^N |\phi_i(\mathbf{r})|^2. \quad (1.20)$$

Equations (1.19) can be solved self-consistently, by arbitrarily choosing a trial function $\tilde{n}(\mathbf{r})$, diagonalizing the one-particle Hamiltonian $\hat{h} = -\frac{1}{2}\nabla^2 + [\varphi(\mathbf{r}) + \mu_{xc}(\tilde{n}(\mathbf{r}))]$, with $\varphi(\mathbf{r})$ from (1.17) and $\mu_{xc}(\tilde{n}(\mathbf{r}))$ from (1.18), then calculating the new $n(\mathbf{r})$ from the eigenvectors of (1.19) and from (1.20), and finally evaluating the total energy. This procedure is repeated until the total energy converges to within the required accuracy.

In spite of being a very crude approximation, the LDA works remarkably well for many solid-state and chemical systems. However, as it neglects long-range exchange-correlation interactions, the LDA often leads to large errors or even unphysical situations⁵. To improve the accuracy of DFT calculations, the exchange-correlation energy per electron can be expressed not only as a function of the local density, but also of the local density gradient⁶: $\varepsilon_{xc}(n(\mathbf{r}), \nabla n(\mathbf{r}))$. This is called the *Generalized Gradient Approximation* (GGA) [12]. There exist several GGA functionals, which differ from

⁵For example, the band gaps of semiconductors and insulators are systematically underestimated [10], while the chemical reaction $\text{H} + \text{H}_2 \rightarrow \text{H}_2 + \text{H}$ is predicted to have a negative activation barrier [11].

⁶Provided that the density is only a slowly varying function—i.e., $|\nabla n|/n^{4/3} \ll 1$.

each other in their parameterization of ε_{xc} as a function of ∇n . Throughout this thesis, we will use the so-called Perdew-Wang 91 functional [13, 14] for GGA calculations.

The diagonalization of the one-particle Hamiltonian in (1.19) is more conveniently carried out by expressing the wavefunctions ϕ_i as series expansions. In solid-state systems, the nuclear potential $v(\mathbf{r})$ possesses the periodicity of the lattice. By using Bloch's theorem, we can then expand the Kohn-Sham orbitals in terms of a plane-wave basis set spanning the discrete space of reciprocal lattice vectors $\{\mathbf{G}\}$:

$$\phi_{\mathbf{k}}(\mathbf{r}) = \sum_{\mathbf{G}} a_{\mathbf{k}+\mathbf{G}} e^{i(\mathbf{k}+\mathbf{G})\cdot\mathbf{r}}. \quad (1.21)$$

Furthermore, as the probability $|a_{\mathbf{k}+\mathbf{G}}|^2$ of finding an electron in the plane-wave state $|\mathbf{k} + \mathbf{G}\rangle$ decays rapidly with its kinetic energy $\frac{1}{2}|\mathbf{k} + \mathbf{G}|^2$, we can assume that wave vectors with amplitude beyond some cutoff value $|\mathbf{G}_{\text{cut}}|$ will contribute negligibly towards the expansion (1.21), thereby reducing the basis set to a finite dimension—albeit at the expense of accuracy. With this in mind, we can rewrite the energy functional $E_v[n]$ in the finite plane-wave expansion (1.21) and make it stationary, to find the Fourier form of the Kohn-Sham equations:

$$\sum_{\mathbf{G}'}^{|\mathbf{k}+\mathbf{G}'|\leq|\mathbf{G}_{\text{cut}}|} \left[\frac{1}{2}|\mathbf{k} + \mathbf{G}'|^2 \delta_{\mathbf{G}\mathbf{G}'} + \varphi(\mathbf{G} - \mathbf{G}') + \mu_{xc}(\mathbf{G} - \mathbf{G}') \right] a_{\mathbf{k}+\mathbf{G}'} \quad (1.22)$$

$$= \varepsilon_{\mathbf{k}} a_{\mathbf{k}+\mathbf{G}},$$

where $\varphi(\mathbf{G} - \mathbf{G}')$ and $\mu_{xc}(\mathbf{G} - \mathbf{G}')$ are the Fourier transforms of $\varphi(\mathbf{r})$ and $\mu_{xc}(n(\mathbf{r}))$. The Hamiltonian in (1.22) is a matrix of finite but large dimensions. Since we are only interested in the N lowest-lying eigenstates, we can consider a tractable submatrix of such a Hamiltonian; the diagonalization of this submatrix yields the lowest-lying energy eigenvalues $\varepsilon_{\mathbf{k}}$ and the expansion coefficients for Equation (1.21).

Once we have diagonalized the Hamiltonian in Equation (1.22), however, we still need to integrate the $\varepsilon_{\mathbf{k}}$ and the $|\phi_{\mathbf{k}}|^2$ over the occupied portion of k -space to get the total energy and the electron density—an intractable task for any physically interesting system. Fortunately, for periodic functions of the wave vector (with periodicity \mathbf{G}), such integration can be reduced to a sum over a finite number of special k -points, with an accuracy that increases with such number [15]. This set of points is usually referred to as the Monkhorst-Pack k -point grid.

To further reduce the time required to perform the self-consistent energy minimization algorithm, we can modify the nuclear potential $v(\mathbf{r})$ to account

for the nodal behavior of the wavefunctions near the nuclei. Since on the one hand core electrons are only marginally affected by valence orbitals, and on the other hand the wavefunction of a valence electron oscillates rapidly near the nucleus, we can replace the strong nuclear potential with an effective *pseudo-potential* that also includes the core electrons, and the valence wavefunctions with pseudo-wavefunctions that have no radial nodes inside a “core” region but that maintain the same overlap integrals. In other words, we replace the nuclei and the core electrons with ions of finite radius, and modify the valence orbitals accordingly. We thus reduce the effective number of electrons in the system and the dimensions of the plane-wave basis set needed to expand the tightly bound core orbitals and the rapidly oscillating valence orbitals. A number of pseudo-potential schemes exist. In the work presented in this report, we have used the Projector Augmented-Wave (PAW) method.

In what has been said so far, the nuclei have been considered fixed at some given position. We have thus made use of the Born-Oppenheimer approximation, decoupling the motion of the nuclei from that of the electrons. If we now wish to compute the equilibrium position of the nuclei (or of the core ions in the pseudo-potential approximation), we need to calculate the forces acting on each ion, using the Hellmann-Feynman theorem, displace the ions accordingly, and then recalculate the total energy functional and the ensuing Hellmann-Feynman forces. This relaxation procedure continues until such forces fall below an arbitrary convergence value.

Chapter 2

State of the Art

The broad topic of interest of the present thesis is the effect of surfaces on the polarization response of ferroelectric materials. The motivation of the work presented herein is the lack of a complete theoretical understanding of switching in ferroelectric capacitors. To date, many aspects of the switching dynamics remain unclear, and among those, first and foremost stands the question of how reverse domains nucleate in a polarized material to which an electric field has been applied opposite to the polarization direction. We will devote the first Section of this Chapter to the state of understanding of the nucleation problem at the time when our research began. Since the nucleation of reverse domains in ferroelectric crystals is observed to originate at the surface of the material, or at the interface with the electrode in the case of capacitors, we will consider in Section 2.2 the correlation between various properties of the surface and the polarization response of the material as discussed in the literature. Closely related to the impact of the surface on the properties of the ferroelectric device is the so-called size effect and the problem of critical thickness for ferroelectricity. A review of work made on these two issues is presented in Section 2.3.

2.1 Domain nucleation in ferroelectrics

The first systematic studies of ferroelectric domains appeared in the late 1940's and early 1950's thanks to the pioneering work of Matthias and Von Hippel [16], Forsbergh [17], and Merz [18, 19] on BaTiO_3 single crystals. It was found that there exist three types of charge-neutral domain boundaries (or domain walls). If we denote by “ c domain” a domain in which the polar axis—which we will take to be in the (001) direction—is perpendicular to the crystal plate surface and by “ a domain” a domain polarized parallel to

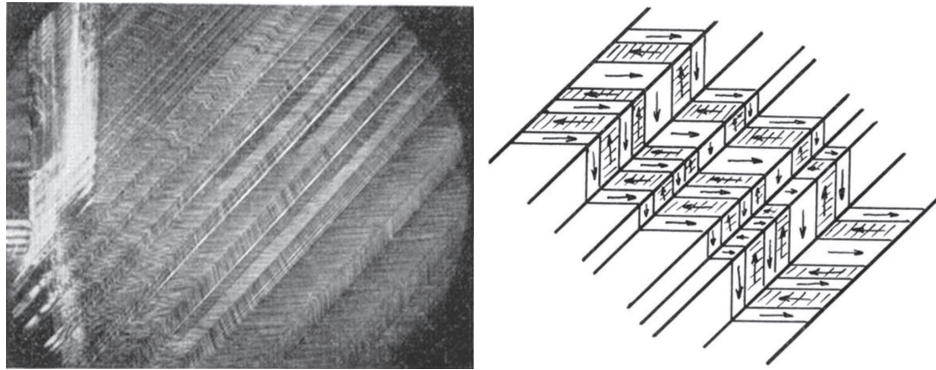


Figure 2.1: The complicated pattern of a and c domains in an unpolarized BaTiO_3 single crystal. Taken from Merz [19].

the plate surface, we can have one of the following:

- c - a domain walls, in which the polar axes for the two domains make a 90° angle between each other, and the domain wall is parallel to a (101) crystallographic plane, thus crossing the crystal at an angle of 45° to the surface;
- a - a domain walls, which are also 90° walls, but parallel to a (110) plane and thus perpendicular to the plate surfaces;
- 180° domain walls, in which the domains are polarized antiparallel to each other.

When there is no applied electric field, the crystal is split into a large number of a and c domains, resulting in a complicated zig-zag pattern of both 90° and 180° domain walls [cf. Figure 2.1]. The a - a and c - a domain arrangements are energetically favorable from the point of view of the total elastic energy of the crystal if the latter is mechanically clamped, whereas the antiparallel arrangement of a or c domains minimizes the total surface charges and therefore the electrostatic energy of the plate. If an electric field is applied to the crystal, say in the $+c$ direction, the 180° domain walls move so as to align the c domains in the direction of the field. If such field is strong enough, the 90° walls also move until the a domains disappear and the whole crystal is polarized in the $+c$ direction.

Another fundamental outcome of the early experimental investigations on ferroelectric domains in BaTiO_3 crystals is the discovery that in the early stages of switching—i.e., in what Merz calls the “low field corner” of the hysteresis loop—it is the nucleation of a large number of new domains, rather than the growth of existing ones, which contributes most to the macroscopic

polarization of the crystal. In other words, it is energetically easier to nucleate new domains within a region of opposite polarization than to enlarge the existing ones—or rather those of them that are polarized in the direction of the field—by a sidewise motion of the domain walls. The new domains nucleate at the surface and at defects in the shape of needles and then grow in the forward direction until they reach the opposite surface. It is therefore the surface nucleation and forward growth of such reverse domains that controls the switching in BaTiO₃ single crystals.

We are then faced with a very common problem in materials science, that of heterogeneous nucleation at a surface. However, if we consider such a problem for an ideal crystal and neglect interactions between the surface and polarization, we arrive at a paradox, in that the probability of thermal activation of the reverse domains at experimentally meaningful values of the applied field is unrealistically small¹. This was shown by Landauer in 1957 [20]. Landauer considered the electrostatic problem of a needle-shaped domain of reversed polarization in a matrix of oppositely polarized material subject to an external electric field [cf. Figure 2.2]. He identified three contributions to the energy of formation of the reverse domain: the work done by the external field source on the crystal, the domain wall energy—i.e., the elastic energy associated with the lattice distortions at the domain boundary, and the electrostatic energy arising from the divergence of polarization at such a boundary. To reproduce the observed needle-like shape of ferroelectric domain nuclei, Landauer assumed that the latter possess the form of half of a prolate spheroid, whose semi-major axis, ℓ , lies along the polar axis of the crystal, and whose base, a circle or radius r , lies on the interface; experimental evidence suggests that $\ell \gg r$. The formation energy for a nucleus of reverse polarization can then be written as:

$$U(r, \ell) = -\frac{4}{3}\pi E_{\text{ext}} P_s r^2 \ell + \frac{\pi^2}{2} \sigma_w r \ell + \frac{16\pi^2}{3\varepsilon_a} P_s^2 \left[\ln \left(\frac{2\ell}{r} \sqrt{\frac{\varepsilon_a}{\varepsilon_c}} \right) - 1 \right] \frac{r^4}{\ell}, \quad (2.1)$$

where E_{ext} is the applied electric field, P_s the spontaneous polarization of the ferroelectric, σ_w the domain wall energy per unit surface, and ε_c and ε_a the components of the dielectric permittivity along the polar axis and perpendicular to it, respectively. The energy (2.1) has a saddle point beyond which the nucleus will grow spontaneously. If we rewrite the formation energy in the simple form:

$$U(r, \ell) = -ar^2\ell + br\ell + c\frac{r^4}{\ell}, \quad (2.2)$$

¹We will show in Chapter 3 that such a paradox can be avoided by considering the coupling between the polarization and the surface.

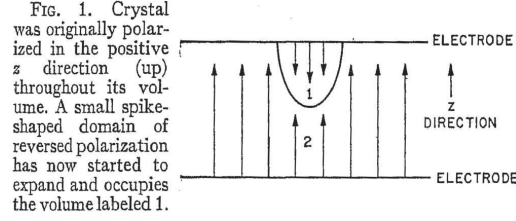


Figure 2.2: A needle-shaped domain of reversed polarization (occupying volume 1) nucleating at the ferroelectric-electrode interface within a matrix of oppositely polarized material (occupying volume 2). The direction of the spontaneous polarization is shown by the arrows. The external electric field is assumed to be applied in the negative z direction. Taken from Landauer [20].

the activation energy for domain growth is then given by

$$U_L = \frac{5^{\frac{5}{2}} b^3 c^{\frac{1}{2}}}{108 a^{\frac{5}{2}}}. \quad (2.3)$$

For a BaTiO_3 plate² at room temperature and under electric fields as high as 100 kV/cm, the Landauer nucleation barrier is virtually insurmountable: $U_L \gtrsim 10^3 k_B T$, which entails a Boltzmann factor $e^{-U_L/k_B T} \lesssim 10^{-434}$. In other words, the probability of thermal activation of reverse domains is practically zero, contrary to experimental evidence. This is known as Landauer's paradox.

Little progress has been made on the resolution of Landauer's paradox in the following decades. A number of authors, notably Kay and Dunn [21], have suggested that the aid of defects or remanent domains might bring the nucleation barrier down to thermally accessible values, but have not provided any quantitative model whose predictions can be tested experimentally. Janovec [22] has shown that in BaTiO_3 single crystals the presence of space charges within a surface layer 0.01 to 1 μm thick favors the formation of needle-shaped anti-parallel domains in an otherwise single-domain structure. Such remanent domains constitute the seeds of domain growth in the switching process. The model of Janovec, which seems to have regrettably fallen into oblivion since, represents, to the best of our knowledge, the most successful attempt to provide an explanation to the puzzle of domain nucleation in BaTiO_3 , though its validity requires that a considerable amount of space charge be available in the surface layer³.

²Typical values for BaTiO_3 crystals under mechanically free boundary conditions are: $\varepsilon_a = 2000 \varepsilon_0$, $\varepsilon_c = 120 \varepsilon_0$, $P_s = 0.26 \text{ m/C}^2$, and $\sigma_w = 7 \times 10^{-3} \text{ J/m}^2$.

³The semiconductor nature of BaTiO_3 might explain the presence of space charge within a surface layer. We will return to this point in Section 2.3 when we discuss the

More recently, Cao *et al.* [23] have performed computer simulations to show that domain nucleation is favored at surfaces. No new qualitative predictions have been offered there, however; in addition, the considered two-dimensional model completely ignores the depolarization energy, which plays a crucial role in the electrostatics of ferroelectric domains and by no means should be neglected. Nucleation scenarios related to additional electron tunneling [24] or surface dead layers [25] have also been discussed in the literature. Yet, as estimates for the nucleation barriers are therein missing, the relevance of those scenarios to any practical situation remains unclear. We will extensively discuss in Chapter 3 a nucleation scenario of general validity which does not encounter any such paradox.

2.2 Interface-related phenomena

The scientific investigations reviewed in the previous Section clearly demonstrate the importance of the surface of the ferroelectric crystal in the nucleation of reverse domains. In the context of electronic applications of ferroelectrics, it is actually the interface between the ferroelectric and the electrode, rather than a free surface, that is usually of interest. As it will become apparent in Chapter 3, the coupling between the interface and the polarization vector has a fundamental impact on the switching properties of the ferroelectric. The main idea is that an interface, or any surface for that matter, breaks all those symmetry elements that change the direction of the normal to the interface. So if the polarization vector has a component perpendicular to the interface, the ferroelectric state with polarization pointing into the interface is in general not equivalent to the state with polarization pointing away from it. In other words, there will be a surface energy term which will depend on the direction of the polarization vector [26, 27], favoring one direction over the other. The coupling of the interface and the polarization thus exerts a *poling effect* on the ferroelectric. In the lowest approximation, this surface energy term is linear in the polarization, ζP per unit surface, where ζ is something of a “local surface field”—i.e., the surface analogue of the electric field in the bulk. Before we can evaluate the effect of ζ on the properties of a ferroelectric plate though, let us see how the presence of a surface can be treated within the framework of the Landau-Ginzburg theory.

The impact of the surface on the ferroelectric properties of a film was first theoretically addressed by Kretschmer and Binder [28]. The starting point of their discussion is the assumption that the surface value of the polarization in a ferroelectric is not affected by the applied electric field as strongly as

issue of critical thickness for ferroelectricity.

that in the bulk. This is consistent with the microscopic argument that the ferroelectric softness of the lattice is somehow suppressed near to the surface. The simplest modeling of this scenario can be performed by assuming that the polarization at the two surfaces of the film is completely blocked. Under such conditions, for a parallel-plate capacitor made of a thin film of ferroelectric sandwiched between two ideal conductors—the polar axis of the ferroelectric lying normal to the plane of the capacitor—the linear polarization response can be described by using the following equation of state:

$$E = \alpha P - \kappa \frac{\partial^2 P}{\partial x^2}, \quad (2.4)$$

with boundary conditions:

$$P(0) = 0, \quad P(h) = 0, \quad (2.5)$$

where P is the polarization associated with the soft mode, and the surfaces of the films are at $x = 0$ and $x = h$. Here, we restrict ourselves for simplicity to the paraelectric phase of the material so that the ferroelectric response is field-induced. Moreover, in what follows we will bear in mind that the relative dielectric permittivity of the material is always large—i.e., $\varepsilon = \alpha^{-1} \gg \varepsilon_0$.

The electric field E appearing in the equation of state (2.4) is the total electric field seen by the ferroelectric. This is the sum of the external applied field, $E_{\text{ext}} = -V/h$, and the depolarizing field due to the gradient of polarization at the interface. The relation between E and E_{ext} can be obtained from the Poisson equation. Taking into account the background contribution to the displacement field ($\varepsilon_b E$, where ε_b is the contribution to the dielectric permittivity from the non-ferroelectric lattice modes of the crystal and from the electronic polarizability [29], $\varepsilon_b \ll \varepsilon$), the Poisson equation is in our case $d(\varepsilon_b E + P)/dx = 0$, leading to the relationship:

$$E = E_{\text{ext}} - \frac{1}{\varepsilon_b}(P - \bar{P}). \quad (2.6)$$

This expression for the total field E can be inserted in Equation (2.4) to obtain a differential equation in P . The solution to such equation, satisfying the boundary conditions (2.5), reads:

$$P(x) = \frac{E_{\text{ext}}}{\alpha} \left(1 - \frac{\cosh \frac{x-h/2}{\xi_1}}{\cosh \frac{h}{2\xi_1}} \right) \frac{1}{1 + 2\frac{\varepsilon}{\varepsilon_b} \frac{\xi_1}{h} \tanh \frac{h}{2\xi_1}}, \quad (2.7)$$

where $\xi_1 = \xi/\sqrt{1 + \varepsilon/\varepsilon_b}$ has the meaning of the scale on which, in this geometry, the polarization changes appreciably near the film surfaces, $\xi =$

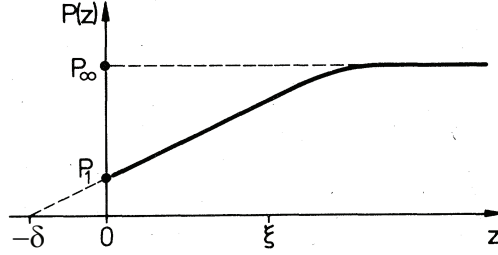


Figure 2.3: Variation of the local polarization $P(z)$ near the vicinity of a surface, located at $z = 0$. δ is the extrapolation length, $P_1 = P(0)$, while P_∞ denotes the bulk value of polarization. Taken from Kretschmer and Binder [28].

$\sqrt{\kappa/\alpha}$ being the so-called *correlation length* of the material evaluated in the paraelectric phase. Typically, ξ rarely exceeds a few nm. Since $\varepsilon_b \ll \varepsilon$, $\xi_1 \approx \xi/\sqrt{\varepsilon/\varepsilon_b} < \xi$, so that, in any situation of practical interest, $\xi_1/h \ll 1$. This consideration can be used to simplify Equation (2.7). By averaging the polarization over the thickness of the film, $\bar{P} = (1/h) \int_0^h P(x) dx$, and by considering the definition of the effective dielectric constant of the film, $\varepsilon_{\text{eff}} = \partial \bar{P} / \partial E_{\text{ext}}$, we get the following approximate expression:

$$\varepsilon_{\text{eff}}^{-1} = \varepsilon^{-1} + \varepsilon_b^{-1} \frac{2\xi_1}{h}. \quad (2.8)$$

This relation corresponds to the in-series connection of the ferroelectric film with two dielectric layers of thickness ξ_1 and dielectric permittivity ε_b . In other words, the surface region with partially suppressed dielectric response behaves as a *passive layer*. This effect is thickness dependent, and due to the smallness of ξ_1 is only felt by thin films.

The discussion above is valid when the polarization at the surface is completely blocked [cf. Equation (2.5)]. The more general situation, where the blocking is not complete, can be simulated by using the following mixed boundary conditions:

$$\delta^{-1} P(0) - \left. \frac{\partial P}{\partial x} \right|_{x=0} = 0, \quad \delta^{-1} P(h) + \left. \frac{\partial P}{\partial x} \right|_{x=h} = 0, \quad (2.9)$$

where δ is the so-called *extrapolation length* of the interface [cf. Figure 2.3]. These conditions interpolate the situation between blocked ($\delta \rightarrow 0$) and free ($\delta \rightarrow \infty$) polarization at the surface. After this modification, the result (2.8) still holds, provided we make the following substitution:

$$\xi_1 \longrightarrow \frac{\xi_1}{1 + \delta/\xi_1}. \quad (2.10)$$

Thus, as one might expect, the weakening of the surface blocking leads to a reduction of the effective passive layer thickness, the passive-layer effect vanishing in the limit of free polarization at the film surface ($\delta \rightarrow \infty$).

A very important phenomenon hidden in Equation (2.8) is the shift of the Curie-Weiss temperature of the phase transition. The anomaly of the permittivity, $\varepsilon = \alpha^{-1}$, observed in bulk crystals when approaching the Curie temperature, in thin films occurs at a different temperature. This is because the presence of the passive layers affects the parameter $\alpha = \varepsilon^{-1}$, which is renormalized to [cf. Equations (2.8) and (2.10)]:

$$\tilde{\alpha} = \alpha + \frac{2\xi_1}{\varepsilon_b h(1 + \delta/\xi_1)}, \quad (2.11)$$

where of course $\alpha = (T - T_0)/\varepsilon_0 C$. Therefore, the Curie-Weiss temperature T_0 is shifted down⁴ by the quantity:

$$\Delta T = \varepsilon_0 C \frac{2\xi_1}{\varepsilon_b h(1 + \delta/\xi_1)}. \quad (2.12)$$

Bratkovsky and Levanyuk [30] extended the theory of Kretschmer and Binder to include the poling effect of the interface in the ferroelectric phase of the material. These authors found that the main impact of the surface field ζ on the relevant properties of the film is a smearing of the ferroelectric phase transition⁵. To prove this, they included the ferroelectric-electrode coupling energy per unit surface, ζP , into the Landau-Ginzburg free energy expression given by Kretschmer and Binder [28]. The inclusion of this coupling term, in the general case of asymmetric interfaces, leads to the following boundary conditions:

$$\delta^{-1} P(0) - \left. \frac{\partial P}{\partial x} \right|_{x=0} = \frac{\zeta_1}{\kappa}, \quad \delta^{-1} P(h) + \left. \frac{\partial P}{\partial x} \right|_{x=h} = \frac{\zeta_2}{\kappa}. \quad (2.13)$$

We see from Equation (2.13) that the effect of the ferroelectric-electrode interface is to pole the film at the surface. The sign of such a poling depends

⁴Incidentally, if the film is thin enough the effective transition temperature can be shifted down to absolute zero, suppressing ferroelectricity in the film. We will return to this point in the following section, where we discuss the critical thickness for ferroelectricity.

⁵A similar result was previously found by Glinchuk and Morozovska [31], who considered the poling effect of the lattice mismatch between the ferroelectric and the substrate. In this case, the smearing of the phase transition is less pronounced, as the effect is proportional to the square of the misfit strain (typically less than 1%). Moreover, the relation between misfit strain and surface polarization in Equations (5) and (7) of Reference [31] is incorrect: it is the latter quantity that is induced by the former via the piezoelectric effect, and not the other way around, so that strain should be multiplied—and not divided—by the piezoelectric coefficient to get the induced polarization!

on the sign of ζ_i . The equation of state of the system in the ferroelectric phase and in the case of a second-order phase transition is:

$$\alpha P + \beta P^3 - \kappa \frac{\partial^2 P}{\partial x^2} = E_{\text{ext}} - \frac{1}{\varepsilon_b} (P - \bar{P}). \quad (2.14)$$

Since the boundary conditions are now asymmetric, then the solution of Equation (2.14) will not be a symmetric function—unlike Equation (2.7). However, the polarization will reach its “bulk value” exponentially fast and over the same distance ξ_1 as before.

Assuming that $\xi_1 \ll \delta$, the dielectric constant of the ferroelectric film is found to be:

$$\varepsilon_{\text{eff}} = \frac{1}{\tilde{\alpha} + 3\beta\bar{P}^2}. \quad (2.15)$$

Not too close to the phase transition, the average polarization in the film can be roughly estimated to be:

$$\bar{P} \approx \frac{1}{\tilde{\alpha}} \left(\frac{\zeta_1 + \zeta_2}{h} \right), \quad (2.16)$$

whereby the effective inverse permittivity of the film has the form:

$$\varepsilon_{\text{eff}}^{-1} \approx \tilde{\alpha} + \frac{3\beta}{\tilde{\alpha}^2} \left(\frac{\zeta_1 + \zeta_2}{h} \right)^2, \quad (2.17)$$

which, in the case of symmetric ferroelectric-electrode coupling ($\zeta_1 = -\zeta_2$), reduces to the result of Kretschmer and Binder—Equations (2.8) and (2.10) in the approximation $\xi_1 \ll \delta$.

Note that the term $3\beta\bar{P}^2$ in the denominator of eq. (2.15) is temperature dependent, through the temperature dependence of $\tilde{\alpha}$ [cf. Equation (2.11)]. If it were not so, its effect would be to further renormalize the Curie-Weiss temperature of the phase transition, which is exactly the effect of the presence of passive layers. But through its temperature dependence, surface poling has the effect of smearing out the phase transition—i.e., of drastically flattening the peak of the dielectric constant as a function of temperature. Using the estimate $\zeta \sim E_{\text{at}} l_{\text{at}}$, we may expect to observe smearing by values as high as ~ 100 K in, e.g., 100 nm-thick films of Ba(Sr,Ti)O₃.

One important remark is in order here. We have seen that in the Landau-Ginzburg theory the properties of ferroelectric thin films with a polarization component normal to the surface rely on the length $\xi_1 \approx \xi / \sqrt{\varepsilon/\varepsilon_b} = \sqrt{\kappa\varepsilon_b}$. Now, in the case of BaTiO₃, $\kappa = 5.1 \times 10^{-10} \text{ Jm}^3/\text{C}^2$ and $\varepsilon_b = 7.35 \varepsilon_0$ [32]. This implies that $\xi_1 \approx 2 \text{ \AA}$. In other words, the spatial scale of variation of the polarization near the surface is less than the lattice spacing. Under such

conditions, a continuum theory such as the Landau-Ginzburg is clearly inapplicable! Hence, while the main qualitative conclusions found by Kretschmer and Binder and by Bratkovsky and Levanyuk are very instructive, their quantitative results should be taken *cum grano salis*.

Moreover, in their treatment of the depolarizing field, the aforesaid authors have treated the electrodes as ideal conductors. However, we know that in real metals the screening of the bound polarization charge is never perfect. The reason for this is the fact that the free charge carriers in the electrode form a layer of finite thickness. The center of mass of the charges in the electrode is then separated by some distance from the bound charge due to polarization in the ferroelectric. In other words, the free charges in the electrode behave as a capacitor connected in-series with the ferroelectric film [33, 34]. Treatment of the electron gas in the electrode in the Thomas-Fermi approximation [35] shows that this capacitor has a capacitance per unit area equal to $\varepsilon_0/\ell_{\text{TF}}$, where ℓ_{TF} is the Thomas-Fermi effective screening length. This leads to the following expression for the apparent dielectric constant of the film:

$$\varepsilon_{\text{eff}}^{-1} = \varepsilon^{-1} + \frac{2\ell_{\text{TF}}}{h}. \quad (2.18)$$

This expression is reminiscent of the result (2.8) found in the case of surface suppression of the polarization. The two phenomena have thus the same effect, as they behave as passive layers that are connected in series with the ferroelectric film and therefore reduce the film's permittivity. It is clear then that Thomas-Fermi screening will induce a further downshift of the Curie-Weiss temperature. However, the two effects cannot be simply superimposed, for the extent of Thomas-Fermi screening is sensitive to the state of polarization at the surface, which in turn depends on the Kretschmer-Binder properties of the system. We will return to this point in Chapter 4.

2.3 Critical thickness for ferroelectricity

We have seen how the size effect due to the surface blocking of polarization on the one hand and to Thomas-Fermi screening on the other leads to a reduction of the effective Curie-Weiss temperature of a ferroelectric thin film. This effect is the larger the smaller the thickness of the film [cf. Equations (2.8) and (2.18)]. Thus, at a given temperature, there exists a value of the film thickness below which the ferroelectric phase becomes thermodynamically unstable. We call this value the *critical thickness* for ferroelectricity of the system. As the size of ferroelectric films in electronic devices is rapidly approaching the limit of a few nanometers, this issue has acquired enormous

technological importance in recent years.

If we consider a ferroelectric crystal with completely uncompensated surface charges $\pm P$, the depolarizing field is equal to $-P/\epsilon_b$, and the shift in the Curie-Weiss temperature is then $-\epsilon_0 C/\epsilon_b \sim 10^4$ K (for normal ferroelectrics) [cf. Equation (2.4) with $E = E_{\text{ext}} - P/\epsilon_b$]. In other words, ferroelectricity is completely suppressed if the depolarizing field is not, at least partially, compensated. Such a compensation can occur by a number of mechanisms, such as the formation of an appropriate domain pattern, the presence of metallic or semiconductor electrodes, the existence of surface conduction states within the ferroelectric, or the interaction with atmospheric ions. All these mechanisms, however, can only achieve partial compensation in the case of a single-domain state, and some bound charge persists on the surfaces which gives rise to a depolarizing field and to the existence of a critical thickness for ferroelectricity.

In 1961, Ivanchik [36] considered the problem of an *in vacuo* BaTiO₃ plate, which he assumed—because of its semiconductor properties—to be partially conducting. He showed that this scenario leads to a thickness dependence of the transition temperature and spontaneous polarization, and to the existence of a critical thickness for ferroelectricity. He estimated this critical thickness to be ~ 20 nm at room temperature. Ivanchik later showed [37] that the difference in workfunction between the two faces of a single-domain ferroelectric plate is larger than the energy gap of the material (~ 3 eV), so that some charge carriers are indeed excited into surface conduction states and partial compensation of the surface polarization is achieved within the ferroelectric. Similarly, surface conduction states can arise at the interface with a semiconductor or an insulator because of the different band structures of the two materials. This scenario was considered by Reiner *et al.* [38], who found that in the case of a Ge/BaTiO₃ system the interface states, as they increase the screening charge available, enhance the stability of the ferroelectric phase. They quantified the effect of the interface states on the critical thickness, which drops from 39 nm when they are neglected to 7 nm when they are included in the picture.

Ten years after the first work of Ivanchik, Batra and Silverman [33] considered the case of a perfectly insulating ferroelectric plate between realistic electrodes, and showed that Thomas-Fermi screening leads to a depression of the Curie-Weiss temperature by the amount $-2\ell_{\text{TF}}C/h$ [cf. Equation (2.18)]. This yields the following expression for the critical thickness of the plate:

$$h_c = \frac{2\ell_{\text{TF}}C}{T_0 - T}. \quad (2.19)$$

For a stress-free BaTiO₃ film between metallic electrodes, $h_c \sim 50$ nm at

room temperature.

However, as the Curie-Weiss temperature is shifted down further because of the surface blocking of polarization [cf. Equation (2.12)], the theoretical critical thickness of a ferroelectric capacitor expected from the Thomas-Fermi and Kretschmer-Binder theories has a value larger than (2.19), i.e.:⁶

$$h_c = \frac{2C}{T_0 - T} \left(\ell_{\text{TF}} + \frac{\varepsilon_0 \xi_1}{\varepsilon_b (1 + \delta/\xi_1)} \right). \quad (2.20)$$

In the case of a BaTiO₃ film between metallic electrodes, ℓ_{TF} and $\xi_1 \varepsilon_0 / \varepsilon_b$ are of the same order of magnitude, and the contribution to h_c from surface blocking of polarization depends on the extrapolation length δ . Since δ can vary from zero to infinity, h_c will be in the range 50–100 nm at room temperature and under mechanically free boundary conditions. Similar values are to be expected for other typical ferroelectric perovskites, such as PbTiO₃. However, this prediction is in stark contrast with experimental evidence: a stable ferroelectric phase has been observed at room temperature in Pb(Zr_{0.2}Ti_{0.8})O₃ films as thin as 4 nm [39], in PbTiO₃ films as thin as 1.2 nm [40], and in BaTiO₃ films as thin as 5 nm [41].⁷ Even if we allow for the mechanical action of the substrate, which corresponds in many cases to a shift of the Curie-Weiss temperature by several hundred degrees [43], the disagreement is still quite remarkable. For example, in the case of Reference [41] (BaTiO₃ films grown on thick SrTiO₃ substrates), the renormalization of T_0 leads to a decrease of the critical thickness by a factor of four, but the predicted value is still more than twice the observed one—and the situation is even worse in the case of PbTiO₃ and PZT.

It should be remarked that, despite the aforementioned shortcomings of the Landau-Ginzburg theory, the estimated order of magnitude of the critical thickness from the work of Batra and Silverman and of Kretschmer and Binder is physically sound for the given scenario—i.e., ferroelectric films between metallic electrodes and with a variable degree of surface blocking of polarization. What is really happening then at the interface that leads to a reduction of the predicted impact of Thomas-Fermi screening and of surface blocking of polarization on the Curie-Weiss temperature? This question has motivated a number of first-principles investigations on the critical thickness

⁶This result is valid only to first approximation, for the surface reduction of polarization affects the extent of Thomas-Fermi screening in the electrode, which in turn affects the downshift of the Curie-Weiss temperature.

⁷It should be mentioned that Li *et al.* [42] have used mean-field theory to evaluate the critical thickness of BaTiO₃ (16 nm at room temperature), PbTiO₃ (2 nm at room temperature), and Pb(Zr_{0.5}Ti_{0.5})O₃ (6 nm at room temperature). However, as they neglected the effect of the depolarizing field, their model is irrelevant to any practical situation.

of various ferroelectric perovskites between a number of metallic, metal-oxide, and semiconducting electrodes.

Ghosez and Rabe [44] have studied the ground state of mechanically free PbTiO_3 films using an effective Hamiltonian parameterized through first-principles calculations. The films were screened by perfectly conducting sheets placed at a distance of a quarter of a lattice constant from the surfaces. The yield of the calculations for films polarized normal to the surface is a critical thickness of three unit cells (1.2 nm) at 0 K⁸. However, the choice of the terms in an effective Hamiltonian is phenomenological at best if not arbitrary, so that the accuracy of the results is questionable. Moreover, the perfectly conducting sheets used to simulate short-circuit boundary conditions are an artifact which raises questions as to the effective validity of the model for practical situations.

To avoid unphysical assumptions a full first-principles treatment is therefore needed. Junquera and Ghosez [45] have considered the problem of BaTiO_3 films sandwiched between SrRuO_3 electrodes and constrained to the in-plane lattice constant of SrTiO_3 . The calculations were performed within density functional theory, using the local density approximation to the Kohn-Sham functional. The ground state of the capacitors was probed using the so-called *frozen-phonon* method, which consists in assuming perfectly rigid electrodes and a polarization state in the ferroelectric given by uniform soft-mode displacements identical to those observed in the bulk material. The authors found that the ground state of the BaTiO_3 films changed from paraelectric to ferroelectric at a thickness of six unit cells (2.4 nm). They also calculated the electrostatic potential across the capacitors, which allowed them to quantify the depolarizing field across the ferroelectric and thus to confirm that it is indeed such field that is responsible for the suppression of ferroelectricity in ultrathin films. Although the pioneering work of Junquera and Ghosez does not suffer from the kind of arbitrary assumptions needed in constructing an effective Hamiltonian, their model is quite a crude representation of a real capacitor, as the ionic displacements are artificially imposed to be uniform in the ferroelectric and zero in the electrode. Such restriction ignores the exact arrangement of the ionic displacements across the capacitor, arising from the surface blocking of polarization on the one

⁸Note that one should be careful when comparing experimental and first-principles values of the critical thickness. While the former are usually obtained at room temperature, the latter are always calculated at absolute zero. As the critical thickness is a temperature-dependent quantity, its value changes by a factor of $1 - 300/T_0$ when calculated at 0 K instead of at room temperature, if we neglect quantum fluctuations. For BaTiO_3 , for example, this means a reduction of roughly 4 times. Thus, a critical thickness of 1.2 nm at 0 K should correspond to a measured value of ~ 5 nm at room temperature.

hand, and from the screening of the bound polarization charge on the other. We will see in Chapter 7 how the ionic displacements induced in the oxide electrodes by the so-called proximity effect have a profound impact on the film properties, leading to enhanced polarization screening and therefore to a reduction of the critical thickness for ferroelectricity.

Chapter 3

Surface-Stimulated Domain Nucleation in Ferroelectrics¹

In Chapter 2, we have discussed the Landauer paradox [20], which concerns the appearance and growth of reverse polarization domains within a matrix of oppositely polarized ferroelectric. Like in other ordered systems, such as ferromagnets (cf. Brown's paradox in [46]) or superfluids and type-II superconductors (cf. the problem of vortex nucleation [47]), the nucleation of such domains in a homogeneous, defect-free material is associated with impractically high energy barriers [20,25,48]. This difficulty is often neglected, by the mere assumption that the nucleation rate is high enough, thanks to defects or to the effect of the surfaces [46]. However, this is not a satisfactory solution of the problem, especially in situations where the evolution of the nucleation process significantly influences some properties of the system. An example of this is the degradation of the switching ability of ferroelectric materials (e.g. so-called polarization fatigue [49,50]), which is thought to be related to the dynamics of nucleation. The demonstration of a realistic nucleation model is of definite importance for the understanding of switching in ferroelectrics. At the same time such a demonstration may be also instructive for understanding analogous phenomena in other ordered systems. In this Chapter, we offer a model of this kind.

We recall from Chapter 2 that Landauer developed a traditional nucleation model dealing with a competition of the bulk and surface contributions to the activation barrier, which is complicated however by an additional electrostatic contribution due to the bound charges at the nucleus boundary. The domains are assumed to nucleate at the ferroelectric-electrode interface, and to grow in the shape of elongated spheroids. The nucleation barrier is found

¹G. Gerra, A. K. Tagantsev, and N. Setter, *Phys. Rev. Lett.* **94**, 107602 (2005).

to be implausibly large ($\gtrsim 10^3 k_B T$), even in the presence of very high electric fields ($\sim 100 \text{ kV/cm}$) [25, 48]. Thus, Landauer’s model reduces essentially to the statement of a paradox: the large discrepancy between the observed and the predicted nucleation rates of reverse domains. Currently growing experimental activity and applications in the field of ferroelectric thin films have motivated interest from theoreticians in this unsolved problem. However, as we have seen, apart from the work of Janovec on the formation of anti-parallel domains within surface space-charge layers in BaTiO_3 single crystals [22], little progress has been made on this issue in the fifty years to follow.

In this Chapter, we consider the classical Landauer model, appended with a ferroelectric-electrode coupling. The cases of homogeneous and random coupling are considered. We quantify the expected reduction of the nucleation barrier to find that it can be essential. We show that the modified model offers the possibility of “cold field switching”—i.e., the existence of a critical applied electric field above which no thermal activation is necessary for nucleation. This phenomenon was not contemplated by previous models, although the clearly non-exponential temperature dependence of the switching dynamics observed experimentally [51–53] strongly suggests a significant non-thermally activated component in ferroelectric switching. Finally, in the case of perovskite-type ferroelectrics with competing tetragonal and rhombohedral ferroelectric phases (the case of primary practical importance) we find that the nucleation is favored near morphotropic phase boundaries.

Our model bears a close resemblance to the one developed by Janovec to explain the presence of anti-parallel domains in an otherwise single-domain single crystal of BaTiO_3 [22]. In Janovec’s model, space charge is assumed to be present in a surface layer with thickness ranging from 0.01 to 1 μm . The field produced by such a space charge is assumed to be large enough to induce the formation of needle-shaped domains polarized in the opposite direction than in the rest of the crystal (the potential difference between the surface and the interior of the crystal was taken by Janovec to be of the order of 1 V, which yields values of the space-charge induced field in the range of 10 to 1000 kV/cm). The electrostatic work done by the space-charge field is the driving force for the appearance of the anti-parallel domains, which are shown to be stable within a given range of dimensions and geometrical aspect ratios. Mathematically speaking, the model we will presently describe coincides with Janovec’s when the thickness of the surface space-charge layer is negligible compared to the height of the anti-parallel domain. However, application of the space-charge model of Janovec in the case of thin films would require numerical values that are much different from those assumed by him. Moreover, our argument is quite general and does not assume the presence of

space charge inside the ferroelectric. Finally, Janovec concerns himself with the stability of the anti-parallel domains, whereas we are interested in their instability—which leads to their spontaneous growth and accordingly to the switching of the polarization in the ferroelectric. We therefore believe that the two models offer quite distinct and complementary information on the physics of domain nucleation and growth.

We start our discussion from the obvious notion that nucleation phenomena can be stimulated at interfaces and defects. For instance, an asymmetry in the polarization dependence of the surface energy of a ferroelectric-electrode interface can lead to a preferred direction of polarization at the interface. This asymmetry is due to the inversion symmetry breaking introduced by the interface. Microscopically, it may originate from the electronic or mechanical properties of the interface and/or the presence of impurities or dislocations. This ferroelectric-electrode coupling can be related to an interface energy density γ that changes its sign according to the polarization direction. In the simplest case, it will be linear in the polarization P_s : $\gamma = \zeta P_s$, where ζ plays the role of a *surface* field conjugate to the order parameter P_s , and can be treated as a *local surface field* in the 2-dimensional space of the interface [26, 27].

To evaluate the domain nucleation in the presence of this coupling we incorporate it into the Landauer model. Though the nucleus shape is not optimized in this model, we believe that the qualitative features of domain nucleation obtained below are reasonable. Specifically, we consider the formation energy of ferroelectric domains in the shape of prolate semi-spheroids (base radius r , height ℓ) with an external electric field E_{ext} normal to the electrodes, which has the form:

$$U(r, \ell) = -ar^2\ell + br\ell + c\frac{r^4}{\ell} - dr^2, \quad (3.1)$$

where:

$$\begin{aligned} a &\equiv \frac{4}{3}\pi E_{ext}P_s, & b &\equiv \frac{\pi^2}{2}\sigma, & d &\equiv \pi\zeta P_s = \pi\gamma, \\ c &\equiv \frac{16\pi^2}{3\varepsilon_a}P_s^2 \left(\ln \left[\frac{2\ell}{r} (\varepsilon_a/\varepsilon_c)^{\frac{1}{2}} \right] - 1 \right) \cong \frac{16\pi^2}{3\varepsilon_a}P_s^2. \end{aligned} \quad (3.2)$$

The first term in (3.1) is the energy gained by the domain upon reversal of the spontaneous polarization P_s (which is assumed to be normal to the electrodes), the second is the energy associated with the creation of the domain boundary (σ is the domain wall energy density), the third term is the depolarizing energy due to the divergence of polarization at the domain boundary

(ε_a and ε_c are the components of permittivity perpendicular and parallel to P_s respectively), and the fourth term is the ferroelectric-electrode interface energy. The parameter c in (3.2), which is accurate in the limit $\ell \gg r$, has only a very weak dependence on ℓ and r ; it will be considered as constant when taking derivatives.

Analysis of the stationary points of U needed for further discussion is straightforward. It is easy to see that the energy (3.1) has a global minimum with respect to ℓ at:

$$\ell = \sqrt{\frac{cr^3}{b-ar}}. \quad (3.3)$$

Substituting (3.3) into (3.1) we get for the radius dependence of the nucleus energy:

$$\frac{U(x)}{U_L} = \sqrt{6}x^2 \left[\sqrt{x \left(1 - \frac{5}{6}x\right)} - \sqrt{\frac{6}{5}\theta} \right], \quad (3.4)$$

where

$$\theta \equiv \frac{d}{2b} \sqrt{\frac{a}{c}}, \quad x \equiv \frac{r}{r_L} = \frac{6a}{5b}r. \quad (3.5)$$

U_L and r_L are the activation energy [cf. Equation (2.3)] and critical radius for nucleation from Landauer's model:

$$U_L = \frac{5^{\frac{5}{2}}b^3c^{\frac{1}{2}}}{108a^{\frac{5}{2}}}, \quad r_L = \frac{5b}{6a}. \quad (3.6)$$

Figure 3.1 shows a plot of $U(x)$ for different values of the parameter θ . In the Landauer model, where $\theta = 0$, we have a local minimum at $r = \ell = 0$ and a saddle point at r_L . For non-zero values of θ , the point $x=0$ becomes unstable, the local minimum U_{min} is shifted to the right and the local maximum U_{max} to the left, while the activation energy, $\Delta U = U_{max} - U_{min}$, is decreased [Figure 3.1(b)]. Here, $U_{min} = U(x_{min})$ and $U_{max} = U(x_{max})$, where x_{min} and x_{max} are the positive roots of equation:

$$\frac{5\sqrt{5x(1-x)}}{4\sqrt{6-5x}} = \theta. \quad (3.7)$$

When the parameter θ exceeds its critical value:

$$\theta_c = \frac{\sqrt{14\sqrt{21}-46}}{8} \cong 0.533, \quad (3.8)$$

Equation (3.7) has no positive roots and the activation barrier disappears [Figures 3.1(c) and (d)]. Unlike the classical Landauer model, we arrive at

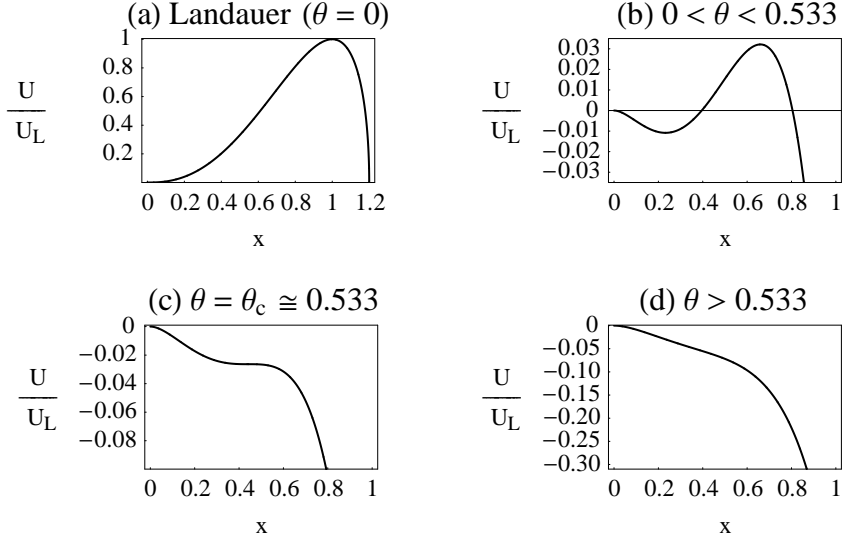


Figure 3.1: The effect of parameter θ on the domain energy (normalized to the Landauer activation energy U_L). The nucleation barrier and critical size x_{max} both decrease with increasing θ values.

the situation where at applied fields corresponding to the condition $\theta > \theta_c$ the nucleation barrier is completely suppressed.

It is instructive to express θ in terms of the anisotropy factor $\eta \equiv \varepsilon_a/\varepsilon_c$ and the thermodynamic coercive field $E_c^{trm} \equiv P_s/3\sqrt{3}\varepsilon_c$, the field at which the anti-parallel orientation of the polarization relative to the field becomes absolutely unstable² [54]:

$$\theta = k \frac{\gamma}{\sigma} \sqrt{\eta \frac{E_{ext}}{E_c^{trm}}}, \quad (3.9)$$

where $k \equiv \left(2\sqrt{3}\sqrt{3\pi^3}\right)^{-1} \cong 0.0394$.

Figure 3.2 is a plot of the activation energy $\Delta U = U_{max} - U_{min}$ (normalized to the Landauer value) as a function of the physical quantities appearing in (3.9)—we do not present the corresponding cumbersome expression. It is evident that as well as by the external electric field, nucleation is favored by high values of the ferroelectric-electrode interface to domain wall energy density ratio, γ/σ , and of the anisotropy factor η . The latter, less evident effect

²Here, for simplicity, we use the expression for the case of a second order phase transition.

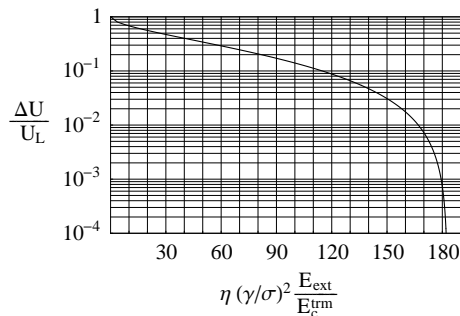


Figure 3.2: Nucleation barrier ΔU (normalized to the Landauer value U_L) as a function of the anisotropy factor η , the external field E_{ext} and the ratio γ/σ .

is related to a reduction of the electrostatic energy which is inversely proportional to the transverse permittivity ε_a —cf. Equation (3.2). From (3.8) and (3.9) we can obtain the applied field needed for total suppression of the nucleation barrier, which we will call zero-temperature critical field $E_c^{T=0}$:

$$\frac{E_c^{T=0}}{E_c^{trm}} \cong \frac{183}{\eta} \left(\frac{\sigma}{\gamma} \right)^2. \quad (3.10)$$

The thick line in Figure 3.3 shows the dependence of $E_c^{T=0}$ on the anisotropy factor η and energy density ratio γ/σ .

In Figure 3.2, we note that the nucleation barrier drops to zero abruptly as the applied field approaches $E_c^{T=0}$. For fields less than 70% of the critical value, $\Delta U \gtrsim 0.1U_L$, implying, for typical values of the relevant parameters, unrealistically low nucleation rates. It follows that, in our model, the finite-temperature critical field is within 30% of $E_c^{T=0}$. Moreover, if nucleation is the limiting factor of switching, then the *coercive field* measured in hysteresis loops is close to this finite-temperature critical field and *does not diverge* when the temperature is decreased—in agreement with experimental findings [51–53].

So far, we have considered a situation where the surface field ζ is homogeneous, which may not be realistic. While small variations in the magnitude of ζ do not alter the qualitative features of our model, fluctuations in the *sign* of ζ might have important consequences. Let us consider the latter type of inhomogeneities. If the typical radius of the regions where ζ is homogeneous, r_0 , is less than or of the order of the Landauer critical radius r_L , than the above theory is clearly inapplicable. The situation where $r_0 \simeq r_L$ requires numerical treatment. However, the case $r_0 \ll r_L$ is readily trackable on the lines of the Imry-Ma statistical approach [55]. Fluctuations in the sign of ζ will result in opposite contributions to the energy—i.e., different

parts of the ferroelectric-electrode interface support different orientations of the polarization. If we take an area of radius $r \gg r_0$, there will on average be an equal number of regions with positive and negative interface energy ($\pm\gamma\pi r_0^2$, depending on the favored direction of polarization). This number is of the order $N \simeq \pi r^2/\pi r_0^2$. Now, from a statistical point of view, it is always possible to find an area where the concentration of, say, positive γ regions is higher, thus favoring nucleation of positive polarization domains. The root-mean-square interface energy of such an area of radius r will be proportional to \sqrt{N} (i.e., $U_{int} = \sqrt{N} \gamma\pi r_0^2 = \gamma\pi r_0 r$), and linear in r . Therefore:

$$U(r, \ell) = -ar^2\ell + br\ell + c\frac{r^4}{\ell} - dr_0r. \quad (3.11)$$

From an analytical point of view, this situation is not qualitatively different from the homogeneous- ζ case. Again, we can rewrite the normalized energy as a function of the dimensionless quantity x , by introducing the same parameters (3.5) and (3.6) as before:

$$\frac{U(x)}{U_L} = \sqrt{6}x \left[\sqrt{x^3 \left(1 - \frac{5}{6}x\right)} - \Theta \right], \quad (3.12)$$

where $\Theta = q\sqrt{\eta}(\gamma r_0/\sigma t_w)(E_{ext}/E_c^{trm})^{\frac{3}{2}}$, $q = (8/5\sqrt{3}\pi^{\frac{5}{3}})^{\frac{3}{2}} \simeq 0.0508$, and $t_w = 6\varepsilon_c\sigma/P_s^2$ is the domain wall thickness from Landau theory [56]. It can be shown that the nucleus energy will have the same characteristics as before, with an unstable stationary point at $r = \ell = 0$, a non-zero local minimum and a saddle point, the latter two converging at $\Theta_c = \sqrt{12\sqrt{2/5}} - 57/8 \simeq 0.682$. The zero-temperature critical field $E_c^{T=0}$ is now modified, and includes a dependence on the typical radius of the homogeneous- ζ regions:

$$\frac{E_c^{T=0}}{E_c^{trm}} \simeq \frac{5.65}{\sqrt[3]{\eta}} \left(\frac{\sigma t_w}{\gamma r_0} \right)^{\frac{2}{3}}. \quad (3.13)$$

Figure 3.3 shows the impact of r_0/t_w on the zero-temperature critical field $E_c^{T=0}$. We can distinguish two regimes. When $r_L \ll r_0$, nucleation is not affected by the inhomogeneity of ζ and the zero-temperature critical field is that given by (3.10) and plotted as a thick line in Figure 3.3. If, on the other hand, $r_L \gg r_0$, the switching cannot originate from homogeneous- ζ regions and $E_c^{T=0}$ is increased (for the same values of η and γ/σ), as given by (3.13)—dashed lines in Figure 3.3. Clearly, the crossover region between the homogeneous and the statistical regime is out of the range of applicability of the present theory, so that in this region the curves should be considered as a guide for the eye.

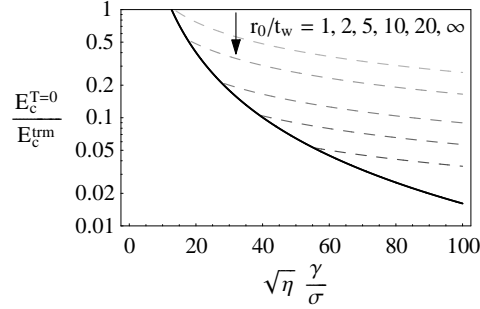


Figure 3.3: Zero-temperature critical ($E_c^{T=0}$) over thermodynamic coercive field (E_c^{trm}), as a function of the anisotropy factor η and of the interface to domain wall energy ratio γ/σ , for increasing values of r_0/t_w (dashed lines). The thick line represents the homogeneous- ζ case, i.e., $r_0/t_w \rightarrow \infty$.

Two issues following from our analysis are worth mentioning. First, nucleation has been found to be favored by a high value of the anisotropy factor η . This implies that the switching can be facilitated in perovskite-type ferroelectrics near *morphotropic phase boundaries*³, where this factor is anomalously high [58]. This prediction corroborates the coercive field reduction in $\text{PbZr}_x\text{Ti}_{1-x}\text{O}_3$ at the tetragonal side of the morphotropic phase boundary [cf. Reference [59] and Figure 3.4].

Second, our model readily provides an exponentially wide spectrum of waiting times for nucleation. It is clear from Figure 3.2 that, in the steep part of the curve (corresponding to a realistic thermoactivation regime), small variations of the system parameters readily lead to orders-of-magnitude variations of the activation barrier, on which the waiting time is exponentially dependent. This result may be relevant to the recent experimental findings on the switching kinetics in ferroelectric thin films, which have been interpreted in terms of this kind of spectrum [60].

Let us now evaluate the strength of the effect predicted by the model. For a rough estimate we use the Landau theory result for the wall energy: $\sigma = t_w P_s E_c^{trm} \sqrt{3}/2$. For the surface field ζ , we use the so-called “atomic” estimate $\zeta \simeq E_{at} l_{at}$ (where $E_{at} \simeq 100 \text{ MV/cm}$ is a typical atomic electric field [61] and l_{at} the lattice constant). This gives us $\sigma/\gamma = \sigma/(P_s \zeta) \simeq (E_c^{trm}/E_{at})(t_w/l_{at})$. Bearing in mind parameters of perovskite ferroelectrics like BaTiO_3 ($E_c^{trm} \sim 500 \text{ kV/cm}$, $t_w \sim 2 \text{ nm}$, $l_{at} \sim 4 \text{ \AA}$) we find that the ratio σ/γ may be as small as 10^{-2} . Thus, according to Equation (3.10), the model can yield a coercive

³This result should not be confused with the predicted reduction of the thermodynamic coercive field near the morphotropic phase boundary demonstrated by M. Iwata and Y. Ishibashi [57].

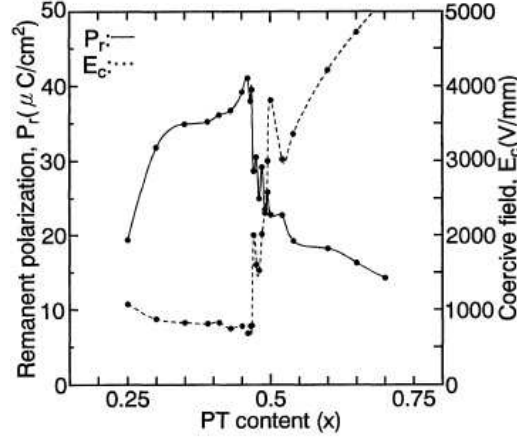


Figure 3.4: Compositional dependence of the remanent polarization, P_r ($\mu\text{C}/\text{cm}^2$), and of the coercive, E_c (V/mm). The coercive field drops abruptly when approaching the morphotropic phase boundary from the tetragonal (PT-rich) side. After Yamamoto [59].

field two orders of magnitude smaller than E_c^{trm} . For a numerical estimate we take room temperature parameters of BaTiO_3 ($P_s = 26 \mu\text{C}/\text{cm}^2$, $\varepsilon_a = 2000 \varepsilon_0$, $\varepsilon_c = 120 \varepsilon_0$, $\sigma = 7 \times 10^{-7} \text{J}/\text{cm}^2$ [20]) to get $E_c^{T=0} \approx 2 \text{kV}/\text{cm}$, according to Equation (3.10) with $\gamma/\sigma = 50$. This estimate holds if $r_0 > r_L \approx 125 \text{nm}$. If $r_0 < r_L$, say 6nm , then according to Equation (3.13): $E_c^{T=0} \approx 18 \text{kV}/\text{cm}$. These estimates show that the model can provide reduction of the coercive field down to typical values for BaTiO_3 single crystals ($\sim 1 \text{kV}/\text{cm}$ [62]).

Chapter 4

Combined First-Principles— Phenomenological Approach to the Size Effect¹

The recent developments in deposition techniques have sparked a surge of interest in thin-film heterostructures. The possibility of miniaturizing layered composites to sub-micron scales offers a plethora of novel applications, but at the same time poses a number of new physical problems that are often difficult to solve. The most obvious of such problems is the size effect: the simple, long-established phenomenological theories that describe the behavior of bulk materials sometimes fail to provide a complete description of low-dimensional systems [63]. The main difficulty lies in the applicability of continuum theories to systems where variations of the relevant physical quantities occur over a length scale comparable to the interatomic distance. In ordered systems such as magnetics, superconductors, or ferroelectrics, continuum theories of the Ginzburg-Landau (GL) type can be safely used when working on a spatial scale controlled by the correlation length, since the latter quantity is typically larger than the interatomic distance. There exists, however, a number of situations where long-range couplings harden the system and the relevant length scale may be considerably reduced to less than the lattice constant of the material. A perfect example of this situation, and one of great practical significance, is the variation of the normal component of the ferroelectric polarization near the interface with an electrode [cf. Section 2.2 and References [28, 64]]. Formally, the GL theory combined with appropriate boundary conditions provides a mathematical description of the

¹G. Gerra, A. K. Tagantsev, and N. Setter, *Phys. Rev. Lett.* **98**, 207601 (2007); A. K. Tagantsev, G. Gerra, and N. Setter, *Phys. Rev. B*, submitted.

size effect in such systems [28, 30, 31]. According to such a theory, in the case of ferroelectrics with a polar axis normal to the interface, the shape of the polarization profile is a result of the interplay between the surface energy (which tends to reduce the surface value of polarization), the gradient energy (which tends to smoothen the variation of polarization over as wide an area as possible), and the depolarizing energy (which tends to maintain the polarization constant). The strength of the depolarizing effect for normal ferroelectrics implies that the polarization profile is very flat and the surface variation of the polarization is confined to a surface region of thickness less than the lattice spacing [29, 65]. Under such a condition a continuum theory such as the GL is not applicable.

In order to avoid such complications, one could in principle treat the problem microscopically—that is, by employing *ab-initio* calculations [45, 66–69]. However, the cost in CPU power and time is a limitation to the maximum size the simulated systems can attain, so that first-principles calculations on experimentally meaningful devices are rarely feasible. Hence, there exists a gap between the microscopic world of *ab-initio* calculations and the macroscopic one of phenomenological theories. It is our purpose in this Chapter to introduce a combined first-principles–phenomenological approach to solving the size effect problem in ferroelectric-electrode systems, an approach which is aimed at bridging such a gap in the theoretical description. The idea is to develop a framework applicable to ultrathin films—so that its parameters can be calculated from first principles—but also to thick films—so that it can be used to describe realistic systems.

4.1 Framework

Let us consider a ferroelectric film of thickness h sandwiched between two short-circuited metallic electrodes. For simplicity, let the film be grown on a substrate that imposes on it a large enough isotropic compressive in-plane strain so that the out-of-plane direction of spontaneous polarization becomes favorable and the ferroelectric phase transition changes its order from first to second². Let P be a spatially uniform quantity, denoting the macroscopic average of the polarization across the ferroelectric film. The free energy of such a system comprises several terms:

- (i) The bulk Helmholtz free energy of the ferroelectric, with order parameters P (the average polarization) and u_i (the strain in Voigt notation);

²This situation can be shown to be realized, for example, in (001) BaTiO₃ films deposited on SrTiO₃ [43, 70], which implies an in-plane misfit strain of about -2% .

- (ii) The depolarizing energy arising from the incomplete screening of the bound polarization charge by the electrodes' free charge carriers;
- (iii) The electrostatic interaction between the polarization and the built-in field arising from the difference in workfunction step between the two interfaces;
- (iv) The surface energy, which can be written as a Taylor expansion in terms of P . (As the interface breaks the inversion symmetry of the ferroelectric, odd-power terms must be taken into account.)³

Since explicit inclusion of the polarization gradient leads to an unphysical result, we implicitly ascribe its effect to the surface terms. The free energy per unit surface of our system therefore reads:

$$\Phi_S = \left(F - \frac{1}{2} \mathbf{E}_{\text{dep}} \cdot \mathbf{P} - \mathbf{E}_{\text{bi}} \cdot \mathbf{P} \right) h + (\zeta_1 - \zeta_2) \mathbf{n} \cdot \mathbf{P} + \frac{1}{2} (\eta_1 + \eta_2) P^2, \quad (4.1)$$

where F is the Helmholtz free energy of the ferroelectric,

$$F = \frac{\alpha}{2} P^2 + \frac{\beta}{4} P^4 + (c_{11} + c_{12}) u_m^2 + \frac{1}{2} c_{11} u_3^2 + 2c_{12} u_m u_3 - q_{11} u_3 P^2 - 2q_{12} u_m P^2, \quad (4.2)$$

and \mathbf{E}_{dep} , \mathbf{E}_{bi} are the depolarizing and built-in field, respectively. The latter quantity is defined as:

$$\mathbf{E}_{\text{bi}} = - \frac{\Delta w_2 + \Delta w_1}{h} \mathbf{n}. \quad (4.3)$$

In the above, $\alpha = (T - T_c)/\varepsilon_0 C$ and β are the Landau double-well-potential coefficients (C being the Curie-Weiss constant), the c_{ij} and q_{ij} the elastic stiffness and electrostrictive tensor components in Voigt notation, Δw_i the workfunction step of interface i , ζ_i and η_i the coefficients of the surface energy expansion for interface i , and \mathbf{n} a unit vector pointing from interface 1 to interface 2. Under the present assumptions, the only nonzero strain components are u_3 along the polar axis and $u_1 = u_2 = u_m$ (the misfit strain due to the substrate) in the plane perpendicular to it. Note that the last term in (4.1) represents the surface tension for the polarized state.

The depolarizing field \mathbf{E}_{dep} is a result of the potential drops, $\Delta\varphi_i$, that appear at each surface because of the unscreened space charge. Under short-circuited boundary conditions, these potential drops must be compensated

³We neglect the surface piezoelectric effect [31], since for realistic values of the misfit strain in the film, its contribution is expected to be only a higher-order correction to the linear contribution of P to the surface energy.

by an equal and opposite potential drop across the ferroelectric:

$$-h\mathbf{E}_{\text{dep}} \cdot \mathbf{n} + \Delta\varphi_1 - \Delta\varphi_2 = 0. \quad (4.4)$$

The potential drops $\Delta\varphi_i$ are taken to be proportional to the surface charge density on the electrodes, $\sigma = \mathbf{D} \cdot \mathbf{n}$, and to the inverse capacitance per unit area of the double electric layers associated with the incomplete polarization screening, λ_i/ε_0 :

$$\begin{aligned} \Delta\varphi_1 &= -\frac{\lambda_1}{\varepsilon_0} \mathbf{D} \cdot \mathbf{n}, \\ \Delta\varphi_2 &= \frac{\lambda_2}{\varepsilon_0} \mathbf{D} \cdot \mathbf{n}. \end{aligned} \quad (4.5)$$

The displacement field is defined as:

$$\mathbf{D} = \varepsilon_b \mathbf{E}_{\text{dep}} + \mathbf{P}, \quad (4.6)$$

ε_b being the background permittivity of the ferroelectric—i.e., the dielectric response of the nonferroelectric modes of the lattice and of the electronic polarizability.

The phenomenological parameters λ_i would indicate the thickness of the double electric layers if their relative permittivities were equal to unity. Hereafter, we will use the term *effective screening length* as a shorthand to refer to them. Such quantities are a property of the particular interface as well as of the electrode, but in general they are also dependent on the polarization direction [cf. Chapter 6], since the sign of the space charge formed at the interface will have an impact on the chemical environment at that interface, and thus on the carriers' surface states which determine the screening properties of the interface. So when we speak of the effective screening length of an interface we mean the average screening length for the two possible polarization directions. Moreover, since the potential drop across the ferroelectric is a combined result of Thomas-Fermi screening and of the sub-lattice-constant surface reduction of polarization, the λ_i implicitly contain both contributions.

Combining Equations (4.4), (4.5) and (4.6) we present the depolarizing field in the form:

$$\mathbf{E}_{\text{dep}} = -\frac{\lambda_1 + \lambda_2}{\varepsilon_0 h + (\lambda_1 + \lambda_2)\varepsilon_b} \mathbf{P}. \quad (4.7)$$

Since the λ_i are typically a fraction of an angstrom [cf. Chapter 5] and $\varepsilon_b \sim 10\varepsilon_0$, we can safely make the following approximation for the depolarizing field:

$$\mathbf{E}_{\text{dep}} = -\frac{\lambda_1 + \lambda_2}{\varepsilon_0 h} \mathbf{P}. \quad (4.8)$$

Now, when the two interfaces are identical⁴ ($\lambda_1 = \lambda_2 = \lambda$, $\Delta w_1 = -\Delta w_2$, $\zeta_1 = \zeta_2$, $\eta_1 = \eta_2 = \eta$), the free energy simplifies significantly. The equation of state for the system ($\partial\Phi_S/\partial P = 0$) in this case gives:

$$\left(\alpha P + \beta P^3 - 2q_{11}u_3P - 4q_{12}u_mP + \frac{2\lambda}{\varepsilon_0 h}P \right) h + 2\eta P = 0. \quad (4.9)$$

All the terms linear in P in the equation of state (4.9) have the effect of renormalizing α , and thus the transition temperature T_c . We need to identify such terms if we want to express the effective transition temperature (T_c^*) and critical thickness (h_c) of the ferroelectric as a function of the interface properties. Now, unlike the misfit strain u_m , the out-of-plane strain component u_3 is not fixed by the action of the substrate, but is determined from the out-of-plane mechanical boundary conditions; in general, it is a function of polarization. With hindsight and for the sake of convenience, we separate the purely mechanical component of u_3 (due to the Poisson ratio of the material) from the component that arises at the phase transition (due to electrostriction). So we write:

$$u_3 = -2 \frac{c_{12}}{c_{11}} u_m + \Delta u_3. \quad (4.10)$$

The first term in Equation (4.10) is constant and therefore affects the transition temperature, while the second term, Δu_3 , depends on the polarization explicitly and must be treated separately. By defining the quantity

$$\alpha' \equiv \alpha + 4q_{11} \frac{c_{12}}{c_{11}} u_m - 4q_{12}u_m, \quad (4.11)$$

we can express the thickness dependence of polarization in the following, simple way:

$$P^2 - \frac{2q_{11}}{\beta} \Delta u_3 = -\frac{1}{\beta} \left(\alpha' + \frac{2\lambda/\varepsilon_0 + 2\eta}{h} \right). \quad (4.12)$$

If the ferroelectric film is fully clamped, Δu_3 is zero for all values of P . If the film is free standing, Δu_3 is proportional to P^2 and leads to a trivial renormalization of β . In the case of first-principles calculations, it is more convenient to fix the dimensions of the whole heterostructure, meaning that the mechanical boundary conditions are mixed, and the explicit dependence of Δu_3 on P is not known *a priori*. However, in the absence of a ferroelectric polarization Δu_3 disappears with P .

A full description of the size effect in ferroelectric thin films with symmetric terminations therefore relies on the knowledge of only two parameters,

⁴The case of asymmetric interfaces will be considered in Chapter 6.

λ and η . These two parameters can be calculated from first principles. If we rewrite Equation (4.12) so as to highlight the thickness dependence of polarization, we can see that the slope of the resulting straight line is just $\lambda/\varepsilon_0 + \eta$:

$$\frac{\partial}{\partial(1/h)} \left(P^2 - \frac{2q_{11}}{\beta} \Delta u_3 \right) = -\frac{2\lambda/\varepsilon_0 + 2\eta}{\beta}. \quad (4.13)$$

The coefficients q_{11} and β can be obtained from experiment or computed from first-principles. Since the value of P , Δu_3 and λ can be extracted from the output of the calculations, as we shall see in Chapters 5 and 6, the evaluation of η follows trivially.

We can see from Equation (4.12) that the shift in T_c for the ferroelectric is the sum of two contributions: the thickness-independent mechanical action of the thick substrate, and the thickness-dependent *size effect* due to imperfect screening and to surface tension. The latter contribution is just

$$\Delta T_c^{\lambda,\eta}(h) = -2C \frac{\lambda + \varepsilon_0 \eta}{h}. \quad (4.14)$$

As the thickness h gets smaller, $\Delta T_c^{\lambda,\eta}(h)$ becomes more negative, T_c^* decreases and so does the polarization. For a given temperature, when the thickness reaches the value

$$h_c = \frac{2\lambda/\varepsilon_0 + 2\eta}{-\alpha'}, \quad (4.15)$$

the spontaneous polarization of the ferroelectric film becomes zero. This is the *critical thickness* for ferroelectricity discussed in Chapter 2, below which no stable ferroelectric state can exist.

We can see from these equations that there are two contributions to the size effect in our systems: one due to the *long-range* electrostatic forces that give rise to the depolarization field—controlled by the effective screening length λ —and another due to the *short-range* coupling between the soft-mode displacements and the electrode—controlled by the parameter η . The separation of the long-range and short-range contributions to the size effect in metal-ferroelectric-metal heterostructures allows to simplify the analysis of the problem and to arrive at a more transparent description of the physics of thin-film ferroelectric capacitors. The next Chapter will be devoted to the evaluation of the two parameters λ and η through ab-initio calculations.

4.2 Applicability

The main feature of our approach is the spatial uniformity of the polarization vector. Such a choice for the shape of the polarization vector was imposed

by the fact that for normal ferroelectrics the polarization varies near the interface over a distance smaller than the lattice spacing, and therefore all effects of such microscopic variation can be included in the surface energy. The spatial scale of variation of the polarization near the interface is given by the quantity [28, 64]

$$\xi_0 = \sqrt{\frac{\kappa\varepsilon_b}{(1 + \varepsilon_b/\varepsilon_f)}}, \quad (4.16)$$

where κ is the coefficient of the gradient term in the GL free energy expansion and ε_f is the permittivity associated with the ferroelectric soft mode. In the case of BaTiO₃, $\kappa = 5.1 \times 10^{10} \text{ J m}^3/\text{C}^2$ [cf. Reference [32]] and $\varepsilon_f \gg \varepsilon_b$. This implies that $\xi_0 \approx \sqrt{\kappa\varepsilon_b} \approx 2 \text{ \AA}$, and a continuum theory such as the GL becomes clearly inapplicable for the description of the spatial variation of the polarization. This justifies our approach where the variation of the polarization at the metal-ferroelectric interface is described by the effective surface energy.

There might exist situations, however, where ξ_0 is indeed larger than the lattice spacing. Let us consider, for example, the case of weak ferroelectrics [71]. These are materials which are characterized by a very weak soft-mode polarity. The link between the soft-mode polarity and the dimensions of ξ_0 can be elucidated from the following simple model arguments. Let us present the total polarization of the ferroelectric P_{tot} as the sum of the ferroelectric (soft-mode) contribution and of the additional one associated with the background permittivity ε_b . The latter contribution we model as that of an optical polar mode (we call it a *hard mode*) whose parameters are those typical for normal dielectrics⁵. Thus we present P_{tot} as:

$$P_{\text{tot}} = \frac{e}{\Omega} (Z_s v_s + Z_h v_h), \quad (4.17)$$

where v_s and v_h are the soft and hard normal mode amplitudes, and Z_s and Z_h are the Born effective charges associated with each mode. For normal ferroelectrics, $1 \lesssim Z_s \sim Z_h$, whereas for weak ferroelectrics, $Z_s \sim 10^{-2}$ or 10^{-3} [cf. Reference [71]], so that $Z_s \ll Z_h$. It can be readily shown that the ferroelectric permittivity and the gradient term depend on the effective charge of the soft mode ($\varepsilon_f \propto Z_s^2$ and $\kappa \propto 1/Z_s^2$), while the background permittivity depends on the effective charge of the hard modes ($\varepsilon_b \propto Z_h^2$). Now, it is seen from Equation (4.16) that a reduction of Z_s from values of order unity to 10^{-2} or 10^{-3} will lead to an increase of ξ_0 up to $\sqrt{\kappa\varepsilon_f}$, which is

⁵Here, we consider for simplicity only one (out-of-plane) component of the polarization and we model the background permittivity with a single hard mode (instead of several polar lattice modes and the electronic contribution).

just the correlation length of the material, ξ . This result can be qualitatively interpreted as follows: with the reduction of the soft-mode effective charge, the additional “electrostatic hardness” of the order parameter vanishes and the spatial scale of the polarization variation tends to the correlation length. The latter quantity may be appreciable on the atomic scale (typically a few nanometers). In this case, the GL theory is applicable to the description of the spatial variation of the polarization. Then, the combined first-principles–phenomenological approach should include the gradient term in the free energy expansion, which implies a solution of the variational problem and the need to extract information about the polarization gradient directly from the output of the calculations. Examples of weak ferroelectric materials are TSCC and $\text{Li}_2\text{Ge}_7\text{O}_{15}$. [71, 72]

A more rigorous treatment of the applicability of our approach can be performed by considering the stability of the spatially varying polarization state against a spatially uniform state, and then by evaluating the range of values of the effective charge associated with the soft mode for which the quantity ξ_0 is appreciably larger than the lattice spacing. This problem does not necessarily imply the solution of the Euler-Lagrange equation for the GL free energy, but can be tackled by solving the associated eigenvalue problem on a small perturbation to the initial polarization state P , as shown by Wang and Woo [73]. This is however beyond the purpose of the present report.

Chapter 5

Separation of Short- and Long-Range Contributions to the Size Effect in Ferroelectrics

The presence of reduced-permittivity interfacial layers in ferroelectric thin-film devices is a longstanding technological problem. Such dead or passive layers reduce the performance of the device, and increasingly so as the thickness of the film gets smaller (hence the expression *size effect*). Though much effort has been put into investigating the dead-layer problem, a thorough understanding of its microscopic details and most of all a solution to such a problem remain an elusive goal. We will now attempt to address this issue.

As it has emerged in the previous Chapters, two known phenomena lie at the origin of the dead-layer effect. The first is the incomplete screening of the bound polarization charge by the electrode's free charge carriers [34]. This effect, which is due to *long-range* electrostatic forces, can be successfully described once cast within the framework of the Thomas-Fermi theory of screening. The second phenomenon is the reduction of polarization at the surface [28], due to the relative “polarization” hardness of an electrode's or substrate's lattice or to atomic relaxations at a free surface. This effect is related to the *short-range* chemical coupling of the atoms at the surface with the electrode or substrate (or to the effect of dangling bonds at free surfaces), and is usually described as the cost in surface energy that must be paid to sustain a finite value of the polarization at the surface. A direct consequence of the surface reduction of polarization is the depolarizing field induced by the divergence of polarization; this provides an additional electrostatic term that does not depend on the screening properties of the electrode.

In Chapter 4, we showed that the size-effect problem in ferroelectric films can be described by using only two physical quantities: the effective screening

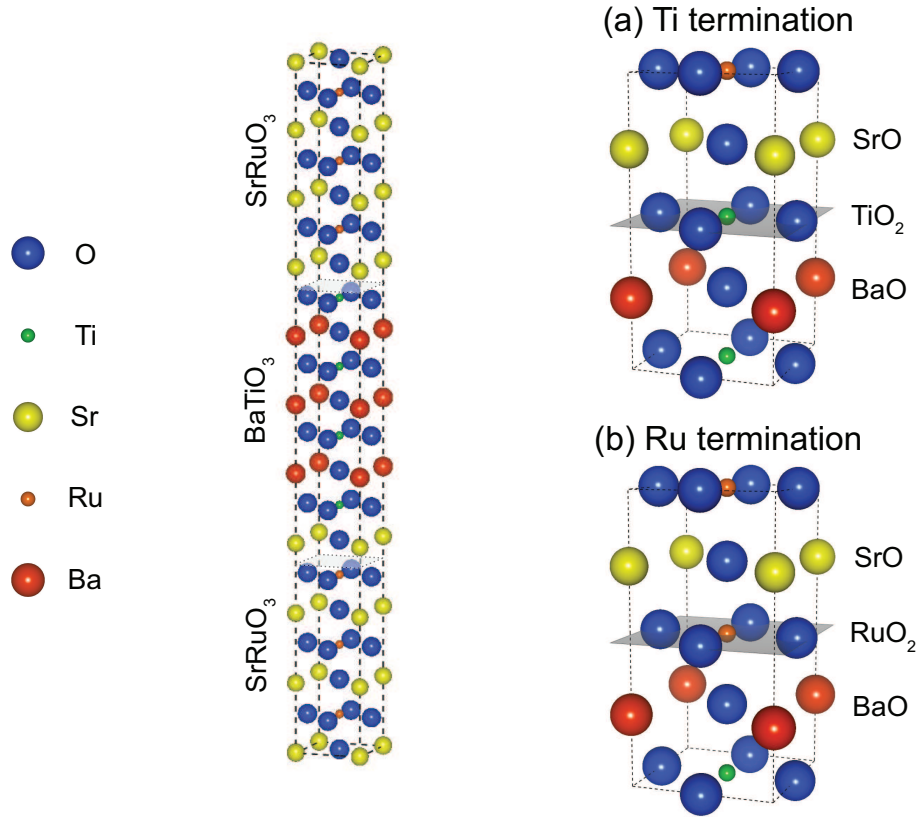


Figure 5.1: An example of the SrRuO₃/BaTiO₃ heterostructures used in the calculations. Two types of terminations can be distinguished: (a) Ti terminations, with an interfacial sequence of atomic planes of the form SrO/TiO₂/BaO, and (b) Ru terminations, with an interfacial sequence of the form SrO/RuO₂/BaO.

length λ —accounting for the long-range electrostatic forces that arise both from Thomas-Fermi screening in the electrode and from the surface variation of polarization—and the surface energy parameter η —accounting for the short-range chemical forces that tend to clamp the polarization at the surface. Although it is believed that for several ferroelectric-electrode systems the most important contribution to the size effect stems from Thomas-Fermi screening [74], the short-range contribution cannot be neglected *a priori*. The work presented in this Chapter provides a quantitative analysis of the two contributions to the size effect, and of their relative importance.

5.1 Calculations

Let us consider the approach developed in Chapter 4. We recall that such an approach involves writing the free energy for the system as a function of the average polarization in the ferroelectric and implicitly including the effect of the polarization gradient into the surface energy terms [cf. Equation (4.1)]. We now apply this scheme to the case of SrRuO₃/BaTiO₃ heterostructures with *symmetric* terminations—the two possible types of termination being Ti [i.e., an interfacial sequence of atomic planes of the type: SrO/TiO₂/BaO, cf. Figure 5.1(a)] or Ru [i.e., SrO/RuO₂/BaO, cf. Figure 5.1(b)]. We perform a series of Density Functional Theory (DFT) calculations on films of different BaTiO₃ thickness (ranging from 3 to 10 unit cells), while the thickness of the SrRuO₃ electrode is fixed at 5 unit cells.

In order to fully understand the properties of the interface, we perform two sets of calculations for each studied system. In the first, we employ the so-called “frozen-phonon” technique [45]. This technique consists in evaluating the equilibrium lattice constants and internal ionic positions of the bulk materials; this will give a centrosymmetric structure for the electrode and a polar one for the ferroelectric, the polarity being characterized by an optic soft phonon mode, to whose amplitude the polarization is directly proportional. A stack of electrode and ferroelectric unit cells of the required height is then constructed, with the electrode ions being fixed to their bulk equilibrium (thus centrosymmetric) positions. The ferroelectric ions are instead displaced by a fraction x of the bulk soft-mode vectors \mathbf{v}_i (where the label i denotes the atomic species), which corresponds to choosing a fraction x of the polarization. The stable polarization state is finally obtained by plotting the total energy of the stack as a function of x , and then by looking for the minima of the energy. This scenario is equivalent to assuming infinitely hard electrodes.

In the second set of calculations, all the ions in the system—including those of the electrode—are fully relaxed until equilibrium is reached [cf. Figure 5.2]. The polarization is then averaged across the ferroelectric. In this second scenario, which implies significantly more time-consuming calculations, the electrode is somewhat “soft”.

The calculations are performed within the generalized-gradient approximation [13, 14] as implemented in the Vienna Ab-initio Simulation Package (VASP) [75, 76], using the projector augmented-wave method for the electron-ion interactions [77]. We employ a 6x6x1 Monkhorst-Pack grid for k -point sampling [15], and a plane-wave energy cut-off of 400 eV. In order to stabilize the tetragonal phase of BaTiO₃ with the polar axis normal to the interface, we impose on the heterostructures a -2% in-plane misfit strain [43], which is

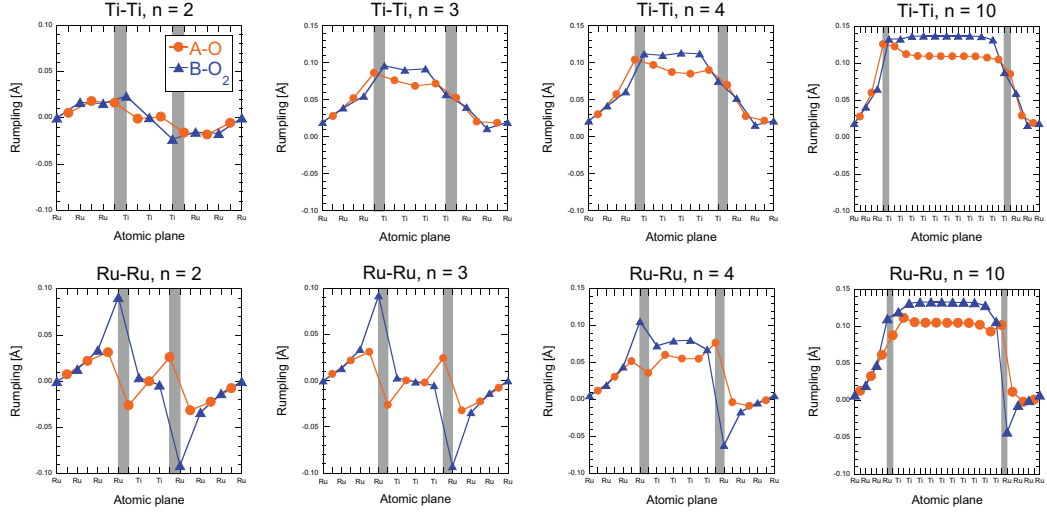


Figure 5.2: The rumplings (i.e., the cation-anion relative displacements within each (001) crystal plane) for SrRuO₃/BaTiO₃ heterostructures of four different thicknesses of the ferroelectric (n is the number of BaTiO₃ unit cells). Both types of symmetric terminations are considered (Ti–Ti and Ru–Ru), under the assumption of a soft electrode. The “A site” of the perovskite structure is occupied either by Sr or by Ba, the “B site” either by Ru or by Ti.

equivalent to the presence of a thick SrTiO₃ substrate. The out-of-plane lattice constant of the SrRuO₃/BaTiO₃ supercell is fixed to its centrosymmetric equilibrium value. The equilibrium ionic positions of the systems with soft electrodes are found by letting all the ions relax until the Hellman-Feynman forces acting on each of them are less than 1 meV/Å.

The calculation of the polarization relies on its microscopic definition as the dipole moment per unit volume of a unit cell: $\mathbf{P} = (e/\Omega) \sum_i Z_i \mathbf{v}_i$ (e being the electronic charge, Ω the unit-cell volume, Z_i and \mathbf{v}_i the Born effective charge and soft-mode displacement of ion i , respectively). Within DFT, the values of the \mathbf{v}_i are obtained by computing the equilibrium positions of the ions, those of the Z_i by using the Berry’s phase approach [78, 79]. The macroscopic polarization of the film is found by averaging over all unit cells.

The coefficients of the GL free energy and the electrostrictive tensor components can be found by varying the polarization or strain and calculating the variation in the energy or polarization of the bulk material. So if we vary the polarization (e.g., by multiplying the equilibrium displacements \mathbf{v}_i by an arbitrary constant), a fit of the change in energy will give us a polynomial whose coefficients are just α , β , etc. [cf. Figure 5.3]. If we vary the strain component u_3 (u_m) and compute the change in the square of the spontaneous

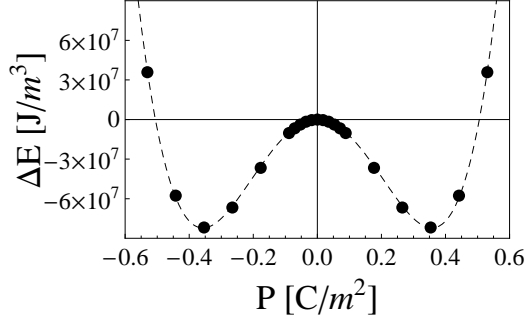


Figure 5.3: The computed Landau double-well potential of fully clamped BaTiO₃. Fitting the data points with an even polynomial yields the Landau coefficients α , β , etc. [cf. Table 5.1].

polarization, a linear fit will yield the tensor component q_{11} (q_{12}). The results of the calculations of the Born effective charges and parameters of the bulk free energy are summarized in Table 5.1. Using Equation (4.13), we can evaluate the sum $\lambda/\varepsilon_0 + \eta$.

The evaluation of λ requires the calculation of the polarization and the depolarizing field across the ferroelectric for a given thickness. From Equation (4.8), with $\lambda_1 = \lambda_2 = \lambda$, we have:

$$\frac{P}{E_{\text{dep}}} = -\frac{\varepsilon_0 h}{2\lambda}. \quad (5.1)$$

The slope of the straight line yields λ . Extracting the value of the depolarizing field from the output of the calculations is straightforward. If we consider the total electrostatic potential felt by an electron in our system, we will observe oscillations due to the periodic structure of the lattice. If, however, we average the potential over, say, a lattice constant, the periodicity will disappear and the macroscopic variations will emerge [80]. We do not expect any variation of the potential within the metal, of course—except in a very thin interfacial layer. The potential drop across such layer must be compensated by an equal and opposite drop across the ferroelectric, since the calculations are performed under short-circuit electrical boundary conditions. The potential drop across the ferroelectric divided by its thickness is just the depolarizing field. Figure 5.5 shows an example of the macroscopically averaged electronic potential across the metal-ferroelectric-metal system.

Table 5.1: The different parameters used in the calculation of λ and η . The coefficient $\alpha' \equiv \alpha + 4q_{11}c_{12}u_m/c_{11} - 4q_{12}u_m$, while Z_{O_I} and $Z_{\text{O}_{II}}$ are the Born effective charges of the oxygens in the BaO and TiO₂ planes, respectively.

Parameter	Value	SI Units
α'	-2×10^9	J m C^{-2}
β	3×10^{10}	$\text{J m}^5 \text{C}^{-4}$
q_{11}	5×10^{10}	J m C^{-2}
Z_{Ba}	2.7	—
Z_{Ti}	7.2	—
Z_{O_I}	-5.7	—
$Z_{\text{O}_{II}}$	-2.1	—

5.2 Results

The results of the calculations for the case of soft electrodes are shown in Figure 5.2, where the rumpling profiles—i.e., the cation-anion relative displacements within each (001) crystal plane—are plotted for four SrRuO₃/BaTiO₃ heterostructures of different thickness (2, 3, 4 and 10 unit cells of BaTiO₃) and for both types of symmetric terminations (Ti–Ti and Ru–Ru). We can see that the zero-temperature critical thickness for ferroelectricity of our system is smaller in the case of Ti–Ti terminations: 3 unit cells of BaTiO₃ as opposed to 4 in the case of Ru–Ru terminations. This is probably related to the remarkably strong poling effect of the Ru interface: the interfacial Ru–O₂ dipole is always directed away from the electrode, even for thicker films, so that when the BaTiO₃ layer is less than 4-unit-cells thick, any long-range ordering is destabilized. What is most striking is that even when the ferroelectric phase is stable, we observe an inversion of the direction of the rumplings in crossing the one interface towards which the polarization vector is pointing (i.e., the right-hand-side interfaces in Figure 5.2). Although such a head-to-head dipole configuration must be evidently chemically more favorable, it is very costly in terms of electrostatic energy, as the two charged layers of the same sign that appear at the two sides of the interface must be screened. In this case, as it emerges from the rumpling profile at the second electrode in the Ru–Ru $n = 4$ plate in Figure 5.2, here we are dealing with a kind of polarization overshoot at the electrode—i.e., the polarization variation at the ferroelectric-electrode interface is *larger* than the value of the spontaneous polarization in the bulk of the film. This implies an elevated value of the effective screening length associated with this interface [cf. Equation (4.5)]. We will return to this point when we discuss the effective screening lengths of our systems.

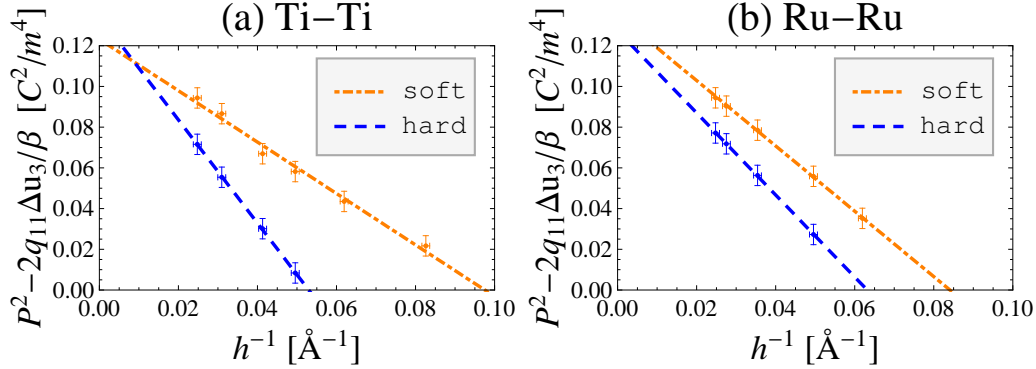


Figure 5.4: The size effect for (a) Ti–Ti and (b) Ru–Ru-terminated heterostructures.

Figure 5.4 shows plots of Equation (4.12) for the SrRuO₃/BaTiO₃ heterostructures with (a) Ti–Ti and (b) Ru–Ru terminations, in the frozen-phonon (*hard* electrode) and full-relaxation (*soft* electrode) methods. In the case of Ti–Ti terminations, the x -intercept tells us that the critical thickness of the heterostructures with hard electrodes is roughly twice the critical thickness of those with soft electrodes [cf. Chapter 7]. The negative slope in the case of hard electrodes is accordingly larger in magnitude, signifying a significantly more pronounced size effect than in the case of soft electrodes. For Ru–Ru terminations, the difference between the two scenarios is smaller, but the size effect is again clearly stronger when the electrode is hard.

Figure 5.5 shows the macroscopically averaged electrostatic potential for a SrRuO₃/BaTiO₃ system with a 10-unit-cell thick BaTiO₃ layer and Ti–Ti terminations. From the slope of the potential within the BaTiO₃ layer we can estimate the depolarizing field. Then, a plot of $|P/E_{\text{dep}}|$ as a function of thickness [Figure 5.6] yields λ [cf. Equation (5.1)]. Note that in the case of Ti–Ti terminations the slope of $|P/E_{\text{dep}}|$ for the hard electrode is smaller than that for the soft electrode by a factor of two, implying a twice-as-large screening length. In the case of Ru–Ru terminations, the situation is reversed, with a slightly larger screening length for the soft-electrode heterostructures. We can relate such a surprising result to the aforementioned polarization overshoot at the RuO₂ termination for soft electrodes, which should result in an elevated value of the effective screening length at this ferroelectric-electrode interface. In the case of hard electrodes, no such overshoot exists. For this reason, in the stack with Ru–Ru terminations, one would indeed expect [in spite of any “*in-situ* screening” argument—cf. Chapter 7] the hard electrode to exhibit a smaller effective screening length than the soft one.

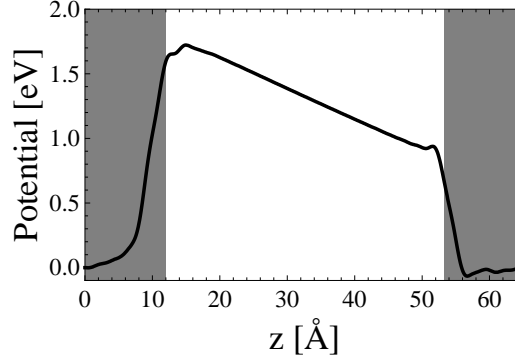


Figure 5.5: The macroscopically averaged electrostatic potential felt by an electron as a function of position along the polar axis, for the heterostructure of ferroelectric thickness $h = 10$ unit cells, Ti–Ti terminations and soft electrodes. The shaded areas represent the region occupied by the electrodes.

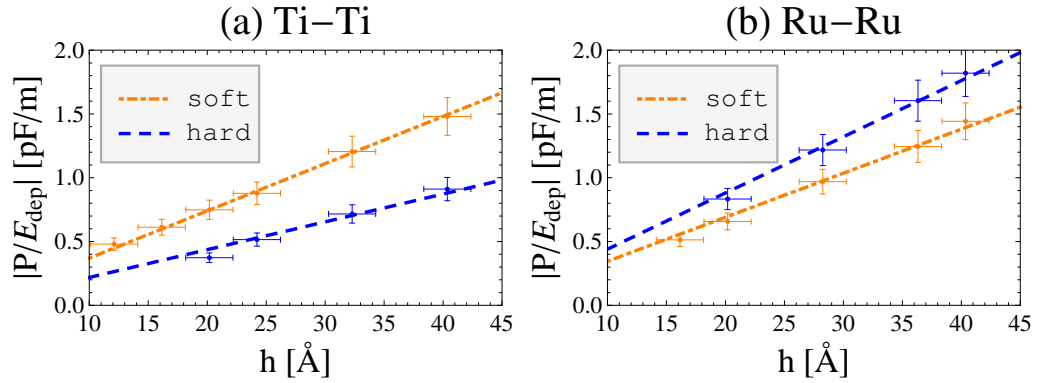


Figure 5.6: $|P/E_{\text{dep}}|$ as a function of thickness for (a) Ti–Ti and (b) Ru–Ru terminations, under soft- and hard-electrode assumptions. According to Equation (5.1), the slope of the lines is $\varepsilon_0/2\lambda$.

Table 5.2: The electrostatic (λ) and nonelectrostatic (η) contributions to the size effect in ferroelectric films, for each type of termination and calculation method.

Parameter	Soft electrode		Hard electrode	
	Ti–Ti	Ru–Ru	Ti–Ti	Ru–Ru
λ	$0.12 \pm 0.01 \text{ \AA}$	$0.13 \pm 0.01 \text{ \AA}$	$0.20 \pm 0.01 \text{ \AA}$	$0.10 \pm 0.01 \text{ \AA}$
$\varepsilon_0\eta$	$\pm 0.01 \text{ \AA}$	$0.01 \pm 0.01 \text{ \AA}$	$0.02 \pm 0.01 \text{ \AA}$	$0.08 \pm 0.01 \text{ \AA}$

The results of the calculations are summarized in Table 5.2. First, we notice that the values of $\varepsilon_0\eta$ are much smaller than the atomic order-of-magnitude estimate: $\varepsilon_0\eta_{\text{at}}$ should be roughly of the order of the typical interatomic distance [30] ($\sim 2 \text{ \AA}$ in our case). In the realistic case of soft electrodes, the difference is two orders of magnitude. Another interesting feature is that the short-range term, $\varepsilon_0\eta$, is always smaller than the long-range one, λ , and significantly so in all cases but one (Ru–Ru terminations with hard electrodes). This justifies the common assumption that the size effect can be identified with the issue of incomplete polarization screening only [45, 74]. Moreover, the value of η in the case of soft electrodes is lower than in the case of hard electrodes, and in one case (Ti–Ti terminations) it is, to within the accuracy of our calculations, close to zero. This result confirms the idea that the beneficial impact of oxide electrodes in reducing the size effect in ferroelectric films can be attributed to the very small opposition to the surface polarization that such class of electrodes offer [81]. The physical reason behind the smallness of $\varepsilon_0\eta$, however, lies beyond our understanding.

Now that we possess quantitative information on the effective screening length λ , we can justify the approximation (4.8) to Equation (4.7), which was based on the assumption that $2\lambda\varepsilon_{\text{b}}/\varepsilon_0$ is small compared to h . For normal ferroelectrics, the background permittivity ε_{b} is typically of the order of $10\varepsilon_0$ [cf. the value $7\varepsilon_0$ in the case of BaTiO_3 , Ref. [32]]. Since $\lambda \sim 0.1 \text{ \AA}$, we have that $\lambda\varepsilon_{\text{b}}/\varepsilon_0 \sim 1 \text{ \AA}$. The relative error involved in our approximation (4.8) is thus: $2\lambda\varepsilon_{\text{b}}/\varepsilon_0 h \lesssim 10\%$.

Chapter 6

Asymmetric Ferroelectric-Electrode Interfaces and Interface Poling¹

The combined phenomenological–first-principles approach introduced in Chapter 4 allows the quantification of the physical parameters underlying the size-effect problem in metal-ferroelectric-metal heterostructures, as we have seen in Chapter 5. The approach was applied to symmetric heterostructures—that is to say, heterostructures with the same termination of the ferroelectric at both interface with the electrode. Now, we wish to treat the case of asymmetric terminations and investigate the effect of the asymmetry on the ferroelectric and piezoelectric properties of the system. We will find that the main effect of the asymmetry, in the absence of external electric fields, is to “pole” the ferroelectric in one particular direction.

6.1 The free energy of asymmetric heterostructures

We consider an electroded and short-circuited single-domain ferroelectric plate of thickness h , whose polar axis lies normal to the ferroelectric-electrode interfaces, the two interfaces being different. The free energy of the system is again given by Equations (4.1), (4.2), (4.3) and (4.8). For the sake of simplicity, we neglect elastic terms² and introduce the quantities $\delta\zeta \equiv \zeta_2 - \zeta_1$

¹G. Gerra, A. K. Tagantsev, and N. Setter, *Phys. Rev. Lett.* **98**, 207601 (2007).

²The effect of the elastic terms in the Landau free energy expansion is a trivial renormalization of the Landau coefficients α and β , as we have amply witnessed in Chapters 4 and 5.

and $\delta w \equiv \Delta w_1 + \Delta w_2$. We can thus rewrite Equations (4.1), (4.2) and (4.3) as

$$\Phi_S = \left(\frac{\alpha}{2} P^2 + \frac{\beta}{4} P^4 - \frac{1}{2} \mathbf{E}_{\text{dep}} \cdot \mathbf{P} - \mathbf{E}_{\text{bi}} \cdot \mathbf{P} \right) h - \delta\zeta \mathbf{n} \cdot \mathbf{P} + \frac{1}{2} (\eta_1 + \eta_2) P^2, \quad (6.1)$$

and

$$\mathbf{E}_{\text{bi}} = -\frac{\delta w}{h} \mathbf{n}, \quad (6.2)$$

while the depolarizing field has still the form (4.8):

$$\mathbf{E}_{\text{dep}} = -\frac{\lambda_1 + \lambda_2}{\varepsilon_0 h} \mathbf{P}. \quad (6.3)$$

Now, if we look at Equations (6.1), (6.2) and (6.3), we can see that there are three terms that depend on the direction of the polarization vector. There are, of course, the electrostatic interaction between \mathbf{E}_{bi} and \mathbf{P} and the surface energy term $-\delta\zeta \mathbf{n} \cdot \mathbf{P}$. And because of the asymmetric interfaces, the effective screening length λ will also be sensitive to the direction of \mathbf{P} . So we have $\lambda_+ = \frac{1}{2}(\lambda_1 + \lambda_2)^+$ for the positive polarization state, and $\lambda_- = \frac{1}{2}(\lambda_1 + \lambda_2)^-$ for the negative state. In terms of the new parameters and for the two polarization states ($P_+ \parallel \mathbf{n}$ and $P_- \parallel -\mathbf{n}$), the free energy can be rewritten as:

$$\begin{aligned} \Phi_S(P_+) &= \left(\frac{\tilde{\alpha}}{2} P_+^2 + \frac{\beta}{4} P_+^4 \right) h + (\delta w - \delta\zeta) P_+ + \frac{P_+^2}{\varepsilon_0} \delta\lambda, \\ \Phi_S(P_-) &= \left(\frac{\tilde{\alpha}}{2} P_-^2 + \frac{\beta}{4} P_-^4 \right) h + (\delta w - \delta\zeta) P_- - \frac{P_-^2}{\varepsilon_0} \delta\lambda, \end{aligned} \quad (6.4)$$

where $\tilde{\alpha} = \alpha + \frac{1}{h}(\eta_1 + \eta_2 + 2\lambda_0/\varepsilon_0)$, $\lambda_0 = \frac{1}{2}(\lambda_+ + \lambda_-)$, and $\delta\lambda = \frac{1}{2}(\lambda_+ - \lambda_-)$.

A full description of asymmetric metal-ferroelectric-metal systems requires knowledge of the asymmetry parameters δw , $\delta\zeta$ and $\delta\lambda$. We shall see that such parameters provide very small corrections to the total energy of the system, so that perturbation theory can be employed to treat the problem. For the sake of convenience, we will introduce the average magnitude of polarization, $P_0 = \frac{1}{2}(|P_+| + |P_-|)$, which is—to first order in the perturbation—the solution to the symmetric equation of state $\tilde{\alpha}P_0 + \beta P_0^3 = 0$. The difference in energy between the two polarization states, $\delta\Phi_S = \Phi_S(P_+) - \Phi_S(P_-)$, can then be related (to first order) to the asymmetry parameters and the average polarization in a simple form:

$$\frac{\delta\Phi_S}{2P_0} = \delta w - \delta\zeta + \frac{P_0}{\varepsilon_0} \delta\lambda. \quad (6.5)$$

Equation (6.5) can be used to extract quantitative information on the asymmetry parameters from the output of first-principles calculations—in particular, from the evaluation of $\delta\Phi_S$ and P_0 for different thicknesses. In order to single out the contributions of δw and $\delta\zeta$ to the offset in $\delta\Phi_S/2P_0$, however, we need further information. Now, the total electrostatic field acting on the ferroelectric film, E , which will be a function of the polarization state, is given by the sum of the depolarizing field and the built-in field E_{bi} :

$$\begin{aligned} E^+ &= E_{\text{dep}}^+ - \frac{\delta w}{h}, \\ E^- &= E_{\text{dep}}^- - \frac{\delta w}{h}, \end{aligned} \quad (6.6)$$

By performing a macroscopic average of the local electrostatic potential [80] across the ferroelectric—another end product of *ab initio* calculations—we obtain the value of E^+ and of E^- . The difference in workfunction step is then given by

$$\delta w = \frac{|E^+| - |E^-|}{2}h - \frac{2P_0\delta\lambda + 2\lambda_0\delta P}{\varepsilon_0}, \quad (6.7)$$

where $\delta P = \frac{1}{2}(|P_+| - |P_-|)$. Using the value of $\delta\lambda/\varepsilon_0$ obtained from Equation (6.5), we can evaluate δw and, consequently, $\delta\zeta$.

For a quantification of the problem, we apply our approach to a set of SrRuO₃/BaTiO₃ heterostructures with asymmetric terminations (RuO₂ and TiO₂), having four different thicknesses of the BaTiO₃ film (8.5, 9.5, 10.5 and 12.5 unit cells) and 4.5 unit cells of the SrRuO₃ electrode. We perform our calculations within the generalized-gradient approximation [13, 14] as implemented in the Vienna Ab-initio Simulation Package (VASP) [75, 76], using the projector augmented-wave method for the electron-ion interactions [77]. We use a 6x6x1 Monkhorst-Pack grid for k -point sampling [15], and a plane-wave energy cut-off of 400 eV. In order to stabilize the tetragonal phase of BaTiO₃ with the polar axis normal to the interface, we impose on it a -2% in-plane misfit strain [43], which is equivalent to the presence of a thick SrTiO₃ substrate. The out-of-plane lattice constant of the SrRuO₃/BaTiO₃ supercell is fixed to its centrosymmetric equilibrium value. The true ground-state ionic configuration of the systems with four different thicknesses is found by letting all the ions relax until the Hellman-Feynman forces acting on each of them are less than 1 meV/Å. The output of the calculations yield the quantities $\delta\Phi_S$, P_+ , P_- , E_+ , and E_- .

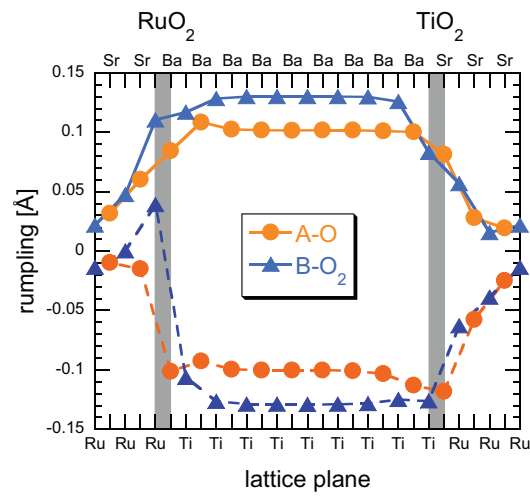


Figure 6.1: Rumpling (i.e., cation-oxygen relative displacement within each atomic layer) profiles along the polar axis for the 4.5SrRuO₃/8.5BaTiO₃ capacitor. The A site (circles) is occupied by the divalent cation (Sr²⁺ or Ba²⁺), while the B site (triangles) by the tetravalent cation (Ru⁴⁺ or Ti⁴⁺). The solid lines represent the rumpling profile for the polarization state of lower energy (P_+), the dashed lines that for the state of higher energy (P_-), while the shaded areas indicate the two interfaces.

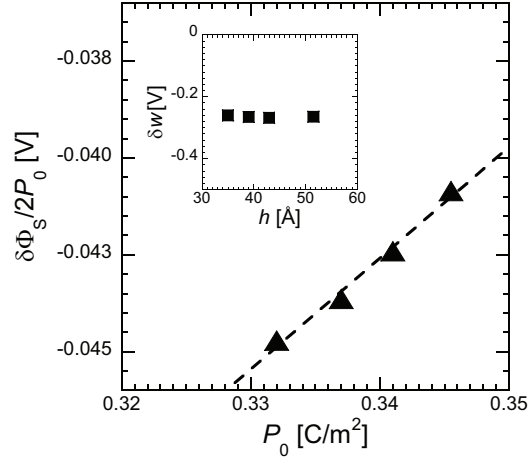


Figure 6.2: $\delta\Phi_S/2P_0$ as a function of P_0 . The slope of the line is $\delta\lambda/\varepsilon_0 = 0.29 \text{ m}^2/\text{F}$, and the y -intercept $\delta w - \delta\zeta = -0.14 \text{ V}$. Inset: difference in workfunction step, δw , as a function of thickness.

6.2 Results

Figure 6.1 shows the rumpling within each atomic layer for the two possible polarization states, for the $4.5\text{SrRuO}_3/8.5\text{BaTiO}_3$ system. The difference in termination breaks the inversion symmetry of the ferroelectric film and lifts the degeneracy for the two states: the state with a polarization vector pointing from the RuO_2 to the TiO_2 termination (P_+) is lower in energy and larger in magnitude. Moreover, the two rumpling profiles are qualitatively different, in that the rumpling for the state of higher energy (P_-) reverses its sign in crossing the RuO_2 -terminated interface.

The asymmetry in termination therefore introduces an energy difference $\delta\Phi_S$ for the two polarization states³, as predicted by Equation (6.5). Figure 6.2 shows a plot of $\delta\Phi_S/2P_0$ as a function of P_0 . According to Equation (6.5), the data points can be fitted by a straight line of slope $\delta\lambda/\varepsilon_0 = 0.29 \text{ m}^2/\text{F}$ and y -intercept $\delta w - \delta\zeta = -0.14 \text{ V}$. By using Equation (6.7), we can then extract the value of δw , and hence that of $\delta\zeta$. We report the three terms that contribute to the energy asymmetry in Table 6.1. Note that δw is thickness independent [inset of Figure 6.2]. This justifies our implicit assumption of weak interface-interface coupling.

We have seen that the two asymmetry parameters δw and $\delta\zeta$ have the effect of poling the ferroelectric film (so-called internal-bias effect). In other

³The calculations yield: $\delta\Phi_S/\Phi_S \sim 5 \times 10^{-5}$, a result which justifies our perturbational approach.

Table 6.1: The three asymmetry parameters of the model.

Parameter	Value
$\delta\lambda$	$(0.026 \pm 0.002) \text{ \AA}$
δw	$(-0.26 \pm 0.03) \text{ V}$
$\delta\zeta$	$(-0.12 \pm 0.04) \text{ V}$

words, their action is equivalent to that of an electric field $-(\delta w - \delta\zeta)/h$. This poling effect—which extends beyond the extreme case of ultrathin films treated in our calculations and applies to thick, realistic capacitors as well—has two obvious consequences: (i) a smearing of the phase transition [30], and (ii) an internal-bias-induced piezoelectric response *above* the transition temperature T_c . Using the results of our calculations, the two effects can be quantified. So if we denote by Γ_κ the full width at half maximum of the permittivity vs. temperature curve, we can plot the evolution of smearing with film thickness for the experimentally meaningful situation of an asymmetrically terminated BaTiO₃ film epitaxially grown between SrRuO₃ electrodes on a thick SrTiO₃ substrate [Figure 6.3(a)]. The extent of smearing can be fitted with reasonable accuracy by a simple power law. Since the maximum of permittivity occurs at T_c , for which $\alpha = 0$, the half maximum above T_c will occur roughly when $\alpha = 3\beta P^2$. This implies that $\Gamma_\kappa \propto P^2$. The value of the polarization is given by the equation of state $\alpha P + \beta P^3 = -(\delta w - \delta\zeta)/h$, with $\alpha = 3\beta P^2$. It follows that $P = [-(\delta w - \delta\zeta)/4\beta h]^{1/3}$, so that $\Gamma_\kappa \propto [-(\delta w - \delta\zeta)/h]^{2/3}$. We use this result to approximate the thickness dependence of smearing via the following analytical expression:

$$\Gamma_\kappa = A \left(-\frac{\delta w - \delta\zeta}{h} \right)^{2/3}. \quad (6.8)$$

By fitting the points obtained from exact numerical calculations, we get: $A \approx 4.5 \times 10^{-3} \text{ K (m/V)}^{2/3}$. The accuracy of the fit is found to be good.

As to the induced piezoelectric response, we can plot [Figure 6.3(b)], for the same BaTiO₃ system at $T = T_c + 50 \text{ K}$, the thickness dependence of the piezoelectric tensor component $d_{33} = 2\kappa_{33}Q_{11}P_3$, where P_3 is the asymmetry-induced polarization component along the polar axis, κ_{33} the dielectric permittivity along the polar axis, and Q_{11} the appropriate electrostrictive tensor component.

An important conclusion can be drawn from our model. The two equations of state of the system ($\partial\Phi_S/\partial P = 0$ for each polarization state), to first order in the perturbation, yield the following expression for the polarization

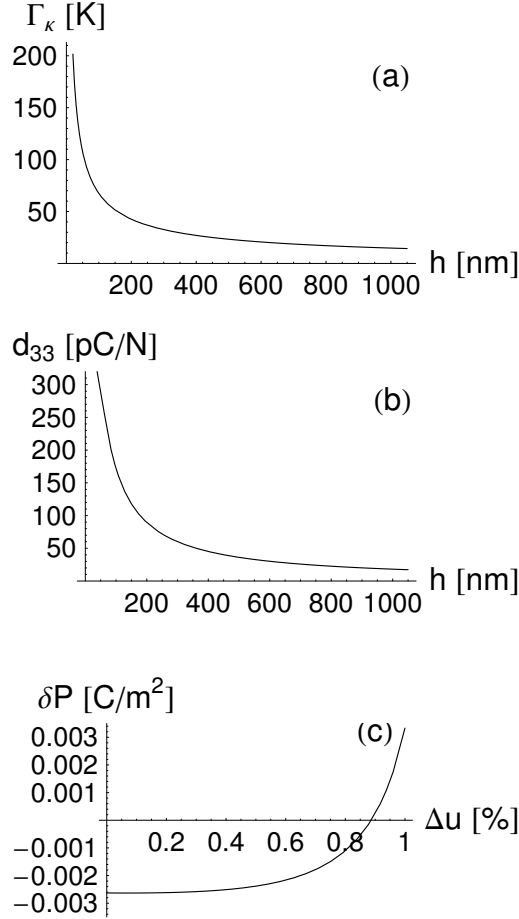


Figure 6.3: (a) Smearing as a function of thickness (Γ_κ is the full width at half maximum of the permittivity vs. temperature curve); (b) asymmetry-induced piezoelectric coefficient d_{33} (calculated at $T = T_c + 50$ K) as a function of thickness; (c) reversal of the sign of δP by application of additional in-plane biaxial strain Δu to a 10-nm film at room temperature. In each case, the effect was evaluated for the case of an asymmetrically terminated BaTiO₃ film epitaxially grown between SrRuO₃ electrodes under 2% compressive in-plane strain. The Landau theory parameters for BaTiO₃ were taken from Reference [82].

asymmetry, $\delta P = \frac{1}{2}(|P_+| - |P_-|)$:

$$\delta P = -\frac{\kappa_{33}}{h} \left(\delta w - \delta \zeta + \frac{2P_0}{\varepsilon_0} \delta \lambda \right). \quad (6.9)$$

Now, $\delta w - \delta \zeta$ and $2P_0 \delta \lambda / \varepsilon_0$ are of opposite sign [cf. Table 6.1], and so is their contribution to the polarization asymmetry. If we can play with the value of P_0 , we can then reverse the sign of δP . This could be accomplished for example by applying strain to the film, since through electrostriction this would vary the absolute value of polarization considerably. For the same BaTiO₃ system (subject to a -2% in-plane misfit strain) considered in Figures 6.3(a) and (b), the reversal of the sign of δP by application of additional in-plane biaxial strain through substrate bending is shown for illustration in Figure 6.3(c). Note that here we speak of reversal of the sign of δP , and not of switching, for it would take a reversal of the sign of $\delta \Phi_S$ to observe the latter phenomenon. For the system under consideration, the term $P_0 \delta \lambda / \varepsilon_0$ in Equation (6.5) is too small for switching to occur, while the factor of 2 in Equation (6.9) makes such term large enough to reverse δP . Switching might become possible, however, if this term were larger due to a larger value of P_0 . Such is the case for, e.g., PbTiO₃-based compounds. Incidentally, the stress-induced switching in Pt/PZT/IrO₂ capacitors that was reported in Reference [83] might be related to the asymmetry effect described in this Chapter.

Chapter 7

In-Situ Polarization Screening in Ferroelectric Capacitors with Oxide Electrodes¹

Ferroelectric oxides are essential components in a large number of applications, from ultrasound medical imaging [84] to non-volatile random access memories [85] and Micro-Electro-Mechanical Systems (MEMS) [86]. Following a general tendency towards miniaturization, ferroelectric-based devices are being shrunk to nanometer scale by growing thin-film capacitor structures. This procedure allows achieving high electric fields from low-voltage sources, but it entails a size effect and ensuing degradation phenomena that limit the performance of the device [50]. As discussed in Chapters 2, 4 and 5, the cause of this size effect is generally believed to be the depolarizing field produced by incomplete screening of the bound polarization charge at the ferroelectric-electrode interface. The presence of such interface is thus equivalent to adding an extra capacitor in series to the ferroelectric, thereby reducing the ability to vary the permittivity and hence the efficiency of the device. In memory applications, such a “surface capacitor” effect is believed to lead to electrical over-stress near the electrodes when cyclically switching the polarization, eventually degrading the switching ability of the film (a phenomenon known as *fatigue* [50]) and impairing the memory’s performance.

Surface effects become the more pronounced the thinner the film. The introduction of an extra capacitor between the metal and the ferroelectric produces a depolarizing field that suppresses the polarization and the permittivity of the film—an effect that grows stronger with decreasing film thickness.

¹G. Gerra, A. K. Tagantsev, N. Setter, and K. Parlinski, *Phys. Rev. Lett.* **96**, 107603 (2006).

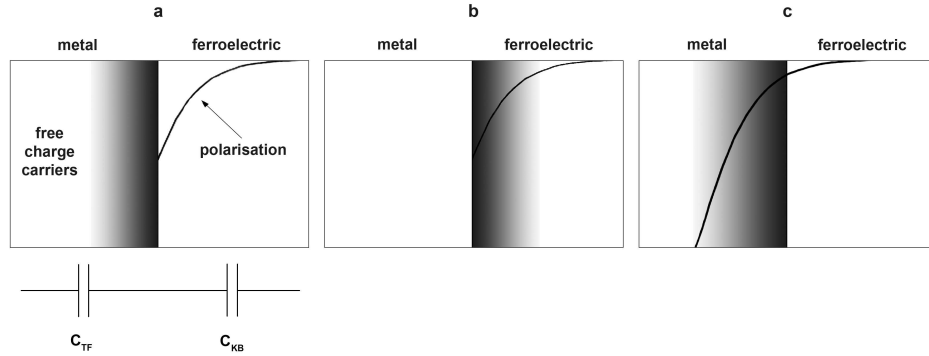


Figure 7.1: The surface-capacitor effect. (a) Thomas-Fermi screening and Kretschmer-Binder effect, each being equivalent to the introduction of a capacitance (C_{TF} and C_{KB}) in series with the ferroelectric. (b) Compensation of the bound charge by the presence of free charge carriers in the ferroelectric, for example as a result of doping or contact phenomena. (c) Penetration of the ionic polarization into the metal, for example as a result of the mechanical relaxation of the electrode ions in response to the ferroelectric distortion of the adjacent lattice. The gradient in shading represents the concentration of free charge carriers, while the solid line represents the absolute value of polarization.

Such phenomenon has provoked speculation in recent years as to whether ferroelectrics have a critical thickness below which ferroelectricity disappears altogether, and whether this limit is intrinsic to the finite size of the system or whether it is imposed by the specific properties of the interface [cf. Chapter 2 and References [39, 40, 45, 66, 67, 87–89]]. In light of the fundamental role played by the surface-capacitor effect in the physics of ferroelectrics and in the performance of coming applications, identifying its origin assumes a significance that goes beyond mere scientific curiosity.

We have seen in Chapters 2 and 4 that there are two distinct possible explanations for the appearance of an additional capacitance at the ferroelectric-metal interface. The first possibility is related to the fact that when free charges in the electrode approach the ferroelectric-electrode interface to screen the bound charge of the ferroelectric, they form a layer of finite thickness (known as the Thomas-Fermi screening length) [34]. Therefore, the center of gravity of the free charges is displaced with respect to the interface, creating a capacitor. On the other hand, the polarization cannot drop abruptly in going from the ferroelectric to the metal (so-called Kretschmer-Binder effect) [28]. For this reason, the center of gravity of the bound charge is shifted away from the metal, creating another capacitor. These two mechanisms, shown schematically in Figure 7.1(a), may act simultaneously as two

back-to-back in-series capacitors.

In an effort to improve the performance of ferroelectric thin-film devices, it was found that the surface-capacitor effect is much weaker when the electrodes are conductive metal-oxides, such as RuO_2 , IrO_2 , or SrRuO_3 . Unlike the case of simple Pt electrodes, for such materials no additional surface capacitor has been revealed by dielectric measurements [90]. This feature is in strong correlation with the essential suppression of degradation effects that is observed when oxide electrodes are used [50, 85]. While the paramount importance of this phenomenon in view of the applications of ferroelectrics is universally recognized, the origin of the beneficial effects of conductive metal-oxide electrodes is still a matter of dispute [cf. reviews in References [29, 50]]. A reasonable approach to the problem is to look for a charge-compensation mechanism that makes the screening more efficient. One possibility is an enhanced concentration of free charge carriers in the first few layers of the ferroelectric [Figure 7.1(b)], for example as a result of doping [50] or of contact phenomena [91]. We can say that in this case the free charges move to where the bound charges are situated, so as to screen them “*in situ*”. The second possibility is the penetration of the bound polarization charges into the electrode. In the case of oxide electrodes, this is made feasible by their ionic structure. We can imagine that the ionic displacements that produce the polarization in the ferroelectric might continue for some distance into the metal-oxide structure, leading again to *in-situ* screening [Figure 7.1(c)]. In this scenario, one can additionally profit from a weaker blocking of polarization at the interface [81]. It is worthy of note that whichever the mechanism behind it, *in-situ* screening can essentially cancel out the destructive effect of the additional surface capacitor, thus explaining the enhanced performance of oxide electrodes.

In this Chapter, we will use the wealth of information derived in Chapter 5 to analyze the second *in-situ* screening scenario. We will show that the latter does indeed take place in BaTiO_3 thin films, hence significantly controlling the size effect.

In the context of density functional theory calculations, we can compare the behavior of a ferroelectric-electrode system in which the electrode ions are blocked (the *hard-electrode* approximation of Chapter 5) with a system in which they are free to move (the *soft-electrode* approximation of Chapter 5), thereby isolating the pure electrostatic effect due to Thomas-Fermi screening from the more complicated problem involving the mechanical relaxation of all the ions. As we saw in Chapter 2, Junquera and Ghosez [45] have focused on the former aspect, modeling the impact of the Thomas-Fermi capacitor on ferroelectricity. Their work is based on the implicit assumption that the ions of the electrode do not react at all to the ionic displacements in the

ferroelectric, and that the latter displacements are homogeneous throughout the material. However, in order to verify whether at a realistic interface the Thomas-Fermi capacitor fully exerts its effect, one can lift the aforementioned assumptions and let the ionic displacements penetrate into the electrode. Incidentally, the importance of allowing the atomic coordinates of the electrode to relax was recognized, but not further investigated, in Reference [67]. If this penetration is important for polarization screening, one expects to find (i) significant ionic displacements within the electrode and (ii) an appreciable reduction of the critical thickness for ferroelectricity in the system. The latter effect arises because better polarization screening implies a reduction of the depolarizing field, which in turn is believed to kill ferroelectricity on decreasing the film thickness. Both predictions have been shown to be correct in Chapter 5. We now wish to further analyze the previous results and attempt to fully understand their implications.

To have a clear comparison with previous results, we have modeled the ferroelectric state of a system identical to that treated by Junquera and Ghosez, and begun by calculating the total energy of the system as a function of the soft-mode distortion amplitude, in the so-called “frozen-phonon” approximation [92] (with the additional assumption that the electrode lattice is perfectly rigid with respect to ionic displacement). Specifically, we have considered SrRuO₃/BaTiO₃/SrRuO₃ sandwich structures with symmetric TiO₂-TiO₂ terminations, where the perovskite ferroelectric is intercalated between two slabs of the perovskite conductor, and assigned the BaTiO₃ ions a given fraction of the computed bulk soft-mode displacement of the relevant atomic species. The total-energy calculations were performed within the generalized-gradient approximation [13, 14], using the Vienna Ab-initio Simulation Package (VASP) [75, 76] and the projector augmented-wave method for the electron-ion interactions [77]. We have used a 6x6x1 Monkhorst-Pack grid for k -point sampling [15], and a plane-wave energy cut-off of 400 eV. The SrRuO₃ and BaTiO₃ in-plane lattice constants were constrained to 3.94 Å (the bulk lattice constant—calculated from first principles for self-consistency—of the fictitious SrTiO₃ substrate [45] that is used to stabilize the tetragonal phase, with the polar axis normal to the interface [43]), while their equilibrium out-of-plane lattice constants were subsequently calculated by minimizing the total energy. The resulting structures were used as the building blocks of the supercell, which consisted of five unit cells of SrRuO₃² and a variable number of BaTiO₃ unit cells. We have considered the simplest

²Calculations performed on the same BaTiO₃ films with six-unit-cell thick SrRuO₃ electrodes showed a negligible effect of the electrode thickness on the relevant properties of the system.

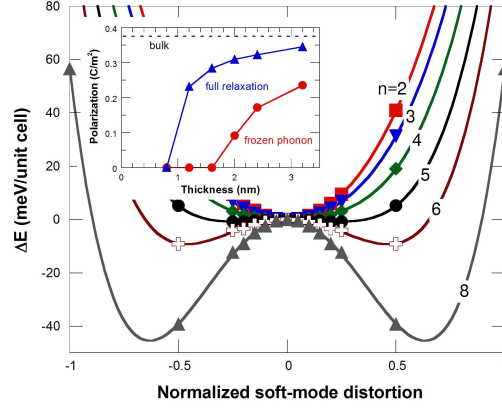


Figure 7.2: The energy change (per unit cell of BaTiO_3) due to a given fraction of the computed bulk ferroelectric soft-mode distortion (in the frozen-phonon approach), for six different thicknesses of the ferroelectric layer (n is the number of unit cells of BaTiO_3). The total energy of the structure in the paraelectric phase is taken as a reference. Inset, average polarization of the ferroelectric layer as a function of thickness, for the frozen-phonon and the full-relaxation data. The polarization was calculated using the computed Born effective charges of bulk BaTiO_3 [78, 79].

computational situation, where the supercell volume is fixed to its centrosymmetric equilibrium value. Such constraint should affect neither the qualitative considerations presented herein nor the obtained value of the critical thickness for ferroelectricity. The extent of the out-of-plane clamping imposed on the structure will somehow modify the absolute value of the spontaneous polarization, which was not, however, the subject of investigation here. The justification of our approach follows from the treatment of clamping effects reported in Reference [43].

Figure 7.2 shows the change in energy effected by a given fraction of bulk soft-mode distortion, for six different thicknesses of the BaTiO_3 layer. The presence of side minima on a particular curve indicates the existence of a ferroelectric instability at such thickness. The minima disappear at a thickness of four unit cells, meaning that the critical thickness for ferroelectricity in this system is 2 nm, in good agreement with the result of Reference [45].

As the next step, we have calculated the true ground-state ionic configuration of the six systems with different thickness by letting all the ions (including those of the electrode) fully relax, until the Hellman-Feynman forces acting on each of them were less than $1 \text{ meV}/\text{\AA}$. The profiles of the rumplings (i.e., the cation-oxygen relative displacements within each atomic layer) thus obtained are shown in Figure 7.3.

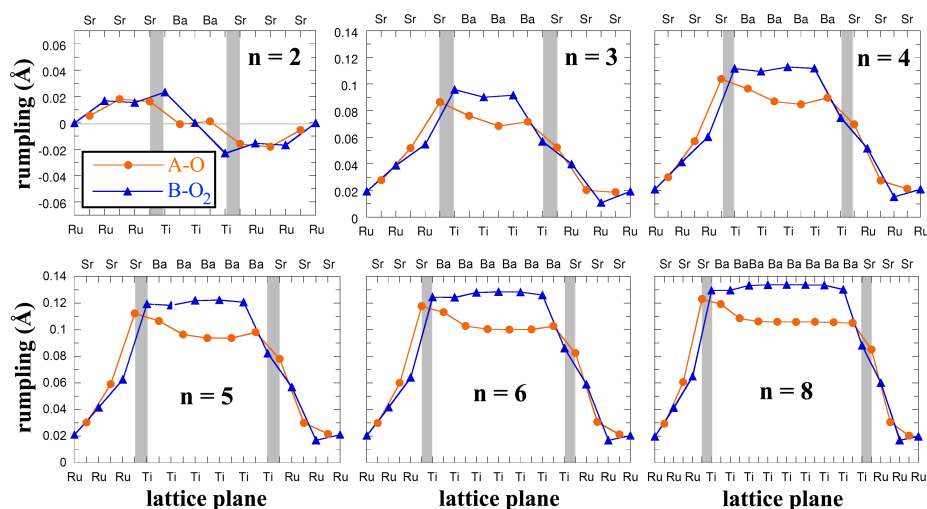


Figure 7.3: The rumpling (i.e., the cation-oxygen relative displacement within each atomic layer) profiles obtained by full minimization of the total energy of the system, for six different thicknesses of the BaTiO_3 layer. The rumpings occur along the polar axis only. The A-site ions are Sr and Ba, while the B-site ions are Ru and Ti.

The foremost result of the calculations is the fact that the ionic displacements penetrate into the metal over a distance of two or three unit cells. Furthermore, the ferroelectric distortions are hardly suppressed as we approach the interfaces, implying little or no surface reduction of polarization. In the case of the thinnest film (two unit cells of BaTiO_3), the rumpling pattern has a mirror-symmetry plane lying in the middle of the ferroelectric layer, and shows a clear antisymmetric poling effect of the two interfaces, which excludes the possibility of a ferroelectric bistability. Such poling effect of the interface is a consequence of its centrosymmetry-breaking action [cf. Chapter 6]. For thicknesses of three unit cells and greater, the mirror symmetry is broken: the rumpings are rather uniform within the ferroelectric film and yield a finite average polarization. This is clearly seen from the inset of Figure 7.2, where, as an illustration, we have plotted the polarization as a function of thickness, using the computed Born effective charges [78, 79] of bulk BaTiO_3 . It follows that the critical thickness for ferroelectricity in BaTiO_3 is three unit cells (~ 1.2 nm), roughly half the value (~ 2 nm) found within the frozen-phonon approximation.

The striking observation of the “softness” of the oxide electrode sheds some light on a fundamental issue concerning ferroelectric thin films. If the ionic displacements associated with the polarization continue into the metal, then those long-range electrostatic effects associated with a nearby-electrode

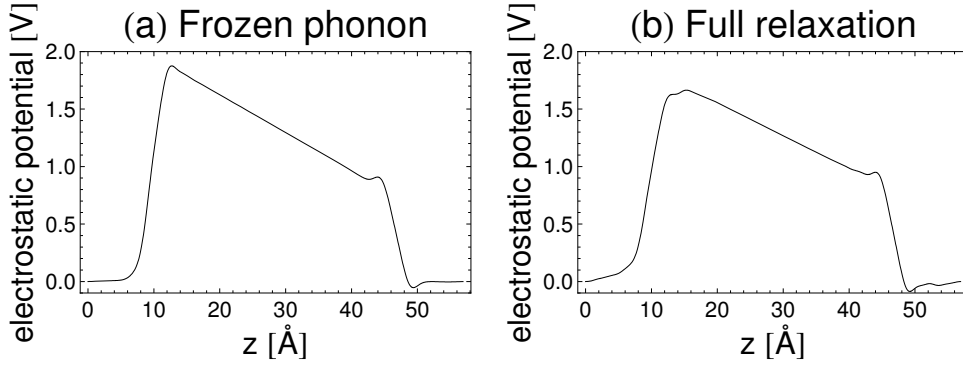


Figure 7.4: The macroscopically-averaged electrostatic potential along the polar axis z , for the system with 8 unit cells of BaTiO_3 under (a) the frozen-phonon and (b) the full-relaxation approximations.

suppression of polarization are heavily reduced for this type of system. In other words, surface-capacitance effects are weaker in this case thanks to the partial screening of the bound polarization charge carried out *in situ* by the electrode's free charge carriers. That such screening is enhanced when the SrRuO_3 interfacial layers are allowed to relax is confirmed by an inspection of the macroscopically-averaged [80] electrostatic potential of the system [cf. Figure 7.4]. By determining the potential drop across the ferroelectric film, we evaluated the depolarizing field [cf. Equation (4.8)],

$$E_{\text{dep}} = -\frac{2\lambda P}{\varepsilon_0 h}, \quad (7.1)$$

and from the calculated average ferroelectric polarization P , we obtained the quantity λ . We found a value of $\lambda \approx 0.2$ for the frozen-phonon data, as opposed to $\lambda \approx 0.1$ for the full-relaxation data [cf. Table 5.2]. Therefore, the lattice softness of SrRuO_3 is responsible for a twofold increase in the screening ability of the electrode, which seems to explain the roughly twofold reduction in the critical thickness for ferroelectricity compared to the frozen-phonon case. The correlation between enhanced screening and stability of the ferroelectric phase suggests that the latter is sensitive to the ionic relaxations because of the more favorable electrostatic state of the resulting relaxed structure, rather than because of the purely mechanical or chemical properties of the interface [cf. Chapter 5].

We have seen that the ionic polarizability of the nearby-interfacial layers of the electrode are essential in stabilizing the ferroelectric phase in BaTiO_3 . However, this may not be a universal property of perovskite ferroelectrics. In a recent first-principles work [67], Sai *et al.* have found that PbTiO_3 , while it retains its ferroelectric character at all thicknesses considered for both

Pt and SrRuO₃ electrodes, shows polarization enhancement in the case of Pt electrodes and polarization reduction in the case of SrRuO₃ electrodes. This suggests that the role of ionic displacements in the electrode is not of primary importance in screening the polarization bound charge for the case of PbTiO₃. The case of SrRuO₃/BaTiO₃/SrRuO₃ structures was also treated by Sai and co-workers, who report absence of ferroelectricity below a thickness of 2 nm. However, the contradiction with our result is only apparent. The point is that in Reference [67] the in-plane lattice constant of the stack is set equal to that of bulk BaTiO₃ at 0 K (3.991 Å). Under such mechanical boundary conditions, BaTiO₃ should have a rhombohedral ground state, as opposed to the artificially stabilized tetragonal state chosen in Reference [45] and in our work. The fact that the atomic relaxation with respect to the out-of-plane coordinates, which was performed in Reference [67], does not reveal ferroelectric minima along the polar tetragonal axis is therefore not evidence of the absence of ferroelectricity.

Chapter 8

Conclusions and Perspectives

We have shown that the coupling between the polarization and the surface of a ferroelectric film has a profound impact on the nucleation process of reverse domains, and therefore on the switching properties of the ferroelectric. The nucleation barrier is reduced when such a coupling is considered, and can even be suppressed altogether when an external field, much smaller than the thermodynamic coercive field, is applied. Our model for reverse domain nucleation enables predictions compatible with several features of switching kinetics in ferroelectrics, such as: (i) the significantly smaller value of the real coercive field compared to the thermodynamic coercive field—thus solving the long-standing coercivity paradox, (ii) the non-diverging temperature dependence of the coercive field upon cooling, (iii) the existence of favorable conditions for nucleation (given by small inhomogeneities in the ferroelectric-electrode interface), with formation of an exponentially wide spectrum of waiting times, and (iv) easier switching close to morphotropic phase boundaries in perovskite-type ferroelectrics.

In order to describe the size effect in ferroelectric thin-film systems, we have developed an approach which combines phenomenological theory and first-principles calculations. Our approach is based on the observation that in the Ginzburg-Landau theory the interfacial variation of the polarization occurs over a distance that is smaller than the lattice spacing; therefore, we take the polarization to be spatially uniform throughout the ferroelectric, and ascribe the effect of the surface variation of polarization to the surface energy terms. Extracting the material parameters of the model from *ab initio* calculations on ultrathin films allows the description of thicker, technologically meaningful systems. From physical arguments we conclude that our approach is fully justified in the case of normal ferroelectrics, for which the soft-mode polarity is strong, whereas for weak ferroelectrics, for which the polarity is much weaker, treatment of the problem should include the gradi-

ent energy, and a solution to the Euler-Lagrange equation for the free energy functional is required.

Our approach shows that the size effect can be described by only two quantities: the effective screening length λ (embodying the long-range electrostatic response of the interface) and the quadratic surface energy coefficient η (embodying the short-range chemical interactions at the interface). In the case of SrRuO₃/BaTiO₃/SrRuO₃ heterostructures with symmetric (i.e., TiO₂-TiO₂ or RuO₂-RuO₂) terminations, the short-range contribution to the size effect is revealed to be less important than the long-range one, as it is often assumed to be the case. The type of termination has a significant impact on the properties of the interface.

In the case of SrRuO₃/BaTiO₃/SrRuO₃ structures with asymmetric (i.e., RuO₂-TiO₂) terminations, we demonstrate and evaluate the poling effect resulting from the interface asymmetry. The observable effects that such an asymmetry induces—namely, smearing of the phase transition, an induced piezoelectric response above T_c , and reversal of the polarization asymmetry by application of biaxial strain—are all found to be appreciable even for realistic film thicknesses, and can in principle be verified experimentally.

Finally, we have demonstrated that perovskite metal-oxides like SrRuO₃ can essentially share the ionic displacements that are responsible for the polarization in ferroelectrics. The effect provides a very efficient mechanism of polarization screening, where the bound charges are screened *in situ* within the electrodes. Such a screening mechanism is shown to lead to an essential reduction of the critical thickness for ferroelectricity in BaTiO₃ (three unit cells). It also offers an explanation for the beneficial impact of oxide electrodes on the switching and dielectric properties of ferroelectric capacitors, which has been extensively documented in experimental reports—cf. the use of IrO₂ electrodes in FeRAM chips to avoid fatigue.

The work presented in this thesis poses a number of questions about the physics of ferroelectric-electrode systems, which in turn suggest potential directions for future research on the topic. First of all, the coupling between the interface and the polarization—which we saw plays a crucial role in stimulating domain nucleation—has not been quantified; only the difference between the coupling energy parameters for the two interfaces, $\delta\zeta$, was calculated. The evaluation of ζ for one interface is not, however, a simple task, for the surface energy comprises contributions from both interfaces. From the point of view of density functional theory, such a task involves the integration of the total-energy functional over half the supercell in real space, a non-trivial effort indeed.

Second, our finding of the predominance of the electrostatic over the chemical contribution to the size effect was only relevant to the case of oxide

electrodes, where the structural affinity with the perovskite ferroelectric is something of a peculiar case. It would be interesting to evaluate the parameters λ and η in the case of metallic electrodes as well, and verify the relative strengths of the two contributions for such type of interface.

Finally, our calculations were performed in the case of an out-of-plane polarization vector, which we know implies depolarizing effects that greatly influence the polarization response. The investigation of the properties of systems with an in-plane polarization vector—which implies the absence of depolarizing fields, and therefore the presence of a single, chemical contribution to the size effect—would be very instructive, especially as far as concerns the interface energy parameter η and the penetration length of the ionic displacements into the electrode.

Bibliography

- [1] Valasek, J. *Phys. Rev.* **15**, 537 (1920).
- [2] Valasek, J. *Phys. Rev.* **17**, 475 (1921).
- [3] Harada, J., Pedersen, T., and Barnea, Z. *Acta Crystallogr. Sect. A* **26**, 336 (1970).
- [4] Devonshire, A. F. *Philos. Mag.* **40**, 1040 (1949).
- [5] Hohenberg, P. and Kohn, W. *Phys. Rev. B* **136**, B864 (1964).
- [6] Dirac, P. A. M. *Proc. Cambridge Philos. Soc.* **26**, 376 (1930).
- [7] Ceperley, D. M. and Alder, B. J. *Phys. Rev. Lett.* **45**, 566 (1980).
- [8] Vosko, S. H., Wilk, L., and Nusair, M. *Can. J. Phys.* **58**, 1200 (1980).
- [9] Kohn, W. and Sham, L. J. *Phys. Rev.* **140**, 1133 (1965).
- [10] Remediakis, I. N. and Kaxiras, E. *Phys. Rev. B* **59**, 5536 (1999).
- [11] Johnson, B. G., Gonzales, C. A., Gill, P. M. W., and Pople, J. A. *Chem. Phys. Lett.* **221**, 100 (1994).
- [12] Perdew, J. P. and Yue, W. *Phys. Rev. B* **33**, 8800 (1986).
- [13] Perdew, J. P. In *Electronic Structure of Solids '91*, Ziesche, P. and Eschrig, H., editors. Akademie Verlag, Berlin (1991).
- [14] Perdew, J. P., Chevary, J. A., Vosko, S. H., Jackson, K. A., Pederson, M. R., Singh, D. J., and Fiolhais, C. *Phys. Rev. B* **46**, 6671 (1992).
- [15] Monkhorst, H. J. and Pack, J. D. *Phys. Rev. B* **13**, 5188 (1976).
- [16] Matthias, B. and Hippel, A. V. *Phys. Rev.* **73**, 1378 (1948).
- [17] Forsbergh, P. W. *Phys. Rev.* **76**, 1187 (1949).

- [18] Merz, W. J. *Phys. Rev.* **88**, 421 (1952).
- [19] Merz, W. J. *Phys. Rev.* **95**, 690 (1954).
- [20] Landauer, R. *J. Appl. Phys.* **28**, 227 (1957).
- [21] Kay, H. F. and Dunn, J. W. *Philos. Mag.* **7**, 2027 (1962).
- [22] Janovec, V. *Czech. J. Phys.* **9**, 468 (1959).
- [23] Cao, W. W., Tavener, S., and Xie, S. M. *J. Appl. Phys.* **86**, 5739 (1999).
- [24] Molotskii, M., Kris, R., and Rosenman, G. *J. Appl. Phys.* **88**, 5318 (2000).
- [25] Bratkovsky, A. M. and Levanyuk, A. P. *Phys. Rev. Lett.* **85**, 4614 (2000).
- [26] Levanyuk, A. P. and Minyukov, S. A. *Fiz. Tverd. Tela (Leningrad) [Sov. Phys. Solid State]* **25**, 2617 (1983).
- [27] Levanyuk, A. P. and Sigov, A. S. *Defects and Structural Phase Transitions*, volume 6 of *Ferroelectricity and Related Phenomena*. Gordon and Breach Science Publishers, Amsterdam, (1988).
- [28] Kretschmer, R. and Binder, K. *Phys. Rev. B* **20**, 1065 (1979).
- [29] Tagantsev, A. K., Sherman, V. O., Astafiev, K. F., Venkatesh, J., and Setter, N. *J. Electroceram.* **11**, 5 (2003).
- [30] Bratkovsky, A. M. and Levanyuk, A. P. *Phys. Rev. Lett.* **94**, 107601 (2005).
- [31] Glinchuk, M. D. and Morozovska, A. N. *J. Phys.: Condens. Matter* **16**, 3517 (2004).
- [32] Hlinka, J. and Marton, P. *Phys. Rev. B* **74**, 104104 (2006).
- [33] Batra, I. P. and Silverman, B. D. *Solid State Commun.* **11**, 291 (1972).
- [34] Tilley, D. R. and Zeks, B. *Ferroelectrics* **134**, 313 (1992).
- [35] Ziman, J. M. *Principles of the Theory of Solids*. Cambridge University Press, Cambridge, 2nd edition, (1972).
- [36] Ivanchik, I. I. *Sov. Phys. Solid State* **3**, 2705 (1962).
- [37] Ivanchik, I. I. *Ferroelectrics* **145**, 149 (1993).

- [38] Reiner, J. W., Walker, F. J., Mckee, R. A., Billman, C. A., Junquera, J., Rabe, K. M., and Ahn, C. H. *Phys. Status Solidi B* **241**, 2287 (2004).
- [39] Tybell, T., Ahn, C. H., and Triscone, J. M. *Appl. Phys. Lett.* **75**, 856 (1999).
- [40] Fong, D. D., Stephenson, G. B., Streiffer, S. K., Eastman, J. A., Auciello, O., Fuoss, P. H., and Thompson, C. *Science* **304**, 1650 (2004).
- [41] Jo, J. Y., Kim, Y. S., Noh, T. W., Yoon, J. G., and Song, T. K. *Appl. Phys. Lett.* **89** (2006).
- [42] Li, S., Eastman, J. A., Vetrone, J. M., Foster, C. M., Newnham, R. E., and Cross, L. E. *Jpn. J. Appl. Phys.* **36**, 5169 (1997).
- [43] Pertsev, N. A., Zembilgotov, A. G., and Tagantsev, A. K. *Phys. Rev. Lett.* **80**, 1988 (1998).
- [44] Ghosez, P. and Rabe, K. M. *Appl. Phys. Lett.* **76**, 2767 (2000).
- [45] Junquera, J. and Ghosez, P. *Nature (London)* **422**, 506 (2003).
- [46] Aharoni, A. *Introduction to the Theory of Ferromagnetism*. Clarendon Press, Oxford, (1996).
- [47] Sonin, E. B. *Physica B* **210**, 234 (1995).
- [48] Tagantsev, A. K. *Integrated Ferroelectrics* **16**, 237 (1997).
- [49] Ozgul, M., Trolier-Mckinstry, S., and Randall, C. A. *J. Appl. Phys.* **95**, 4296 (2004).
- [50] Tagantsev, A. K., Stolichnov, I., Colla, E. L., and Setter, N. *J. Appl. Phys.* **90**, 1387 (2001).
- [51] Xu, F., Trolier-Mckinstry, S., Ren, W., Xu, B. M., Xie, Z. L., and Hemker, K. J. *J. Appl. Phys.* **89**, 1336 (2001).
- [52] Stolichnov, I., Tagantsev, A., Setter, N., Cross, J. S., and Tsukada, M. *Appl. Phys. Lett.* **83**, 3362 (2003).
- [53] Astafiev, K. F., Sherman, V. O., Cantoni, M., Tagantsev, A. K., Setter, N., Petrov, P. K., Kaydanova, T., and Ginley, D. S. *Mat. Res. Soc. Symp. Proc.* **783**, 109 (2004).

- [54] Landau, L. D., Lifshitz, E. M., and Pitaevskii, L. P. *Electrodynamics of Continuous Media*, volume 8. Butterworth-Heinemann, Oxford, 2nd edition, (1995).
- [55] Imry, Y. and Ma, S. *Phys. Rev. Lett.* **35**, 1399 (1975).
- [56] Strukov, B. A. and Levanyuk, A. P. *Ferroelectric Phenomena in Crystals: Physical Foundations*. Springer, Berlin, (1998).
- [57] Iwata, M. and Ishibashi, Y. *Jpn. J. Appl. Phys.* **38**, 5670 (1999).
- [58] Ishibashi, Y. and Iwata, M. *Jpn. J. Appl. Phys.* **38**, 800 (1999).
- [59] Yamamoto, T. *Jpn. J. Appl. Phys.* **35**, 5104 (1996).
- [60] Tagantsev, A. K., Stolichnov, I., Setter, N., Cross, J. S., and Tsukada, M. *Phys. Rev. B* **66**, 214109 (2002).
- [61] Gurevich, V. L. *Transport in Phonon Systems*. North-Holland, Amsterdam, (1986).
- [62] Jona, F. and Shirane, G. *Ferroelectric Crystals*. Macmillan, New York, (1962).
- [63] Jia, C. L., Nagarajan, V., He, J. Q., Houben, L., Zhao, T., Ramesh, R., Urban, K., and Waser, R. *Nat. Materials* **6**, 64 (2007).
- [64] Tagantsev, A. K. and Gerra, G. *J. Appl. Phys.* **100**, 051607 (2006).
- [65] Tagantsev, A. K., Sherman, V. O., Astafiev, K. F., Venkatesh, J., and Setter, N. *J. Electroceram.* **14**, 199 (2005).
- [66] Meyer, B. and Vanderbilt, D. *Phys. Rev. B* **63**, 205426 (2001).
- [67] Sai, N., Kolpak, A. M., and Rappe, A. M. *Phys. Rev. B* **72**, 020101 (2005).
- [68] Dawber, M., Rabe, K. M., and Scott, J. F. *Rev. Mod. Phys.* **77**, 1083 (2005).
- [69] Stengel, M. and Spaldin, N. A. *Nature (London)* **443**, 679 (2006).
- [70] Pertsev, N. A., Zembilgotov, Z. G., and Tagantsev, A. K. *Ferroelectrics* **223**, 79 (1999).
- [71] Tagantsev, A. K., Sinii, I. G., and Prokhorova, S. D. *Izv. Akad. Nauk SSSR Ser. Fiz. [Bull. Acad. Sci. USSR Phys. Ser.]* **51**, 2082 (1987).

- [72] Kadlec, F., Petzelt, J., Zelezny, V., and Volkov, A. A. *Solid State Commun.* **94**, 725 (1995).
- [73] Wang, B. and Woo, C. H. *J. Appl. Phys.* **97**, 084109 (2005).
- [74] Rabe, K. M. *Nat. Nanotechnol.* **1**, 171 (2006).
- [75] Kresse, G. and Furthmuller, J. *Phys. Rev. B* **54**, 11169 (1996).
- [76] Kresse, G. and Furthmuller, J. *Comput. Mater. Sci.* **6**, 15 (1996).
- [77] Kresse, G. and Joubert, D. *Phys. Rev. B* **59**, 1758 (1999).
- [78] Resta, R., Posternak, M., and Baldereschi, A. *Phys. Rev. Lett.* **70**, 1010 (1993).
- [79] Kingsmith, R. D. and Vanderbilt, D. *Phys. Rev. B* **47**, 1651 (1993).
- [80] Baldereschi, A., Baroni, S., and Resta, R. *Phys. Rev. Lett.* **61**, 734 (1988).
- [81] Vendik, O. G. and Zubko, S. P. *J. Appl. Phys.* **82**, 4475 (1997).
- [82] Li, Y. L., Cross, L. E., and Chen, L. Q. *J. Appl. Phys.* **98**, 064101 (2005).
- [83] Gruverman, A., Rodriguez, B. J., Kingon, A. I., Nemanich, R. J., Tagantsev, A. K., Cross, J. S., and Tsukada, M. *Appl. Phys. Lett.* **83**, 728 (2003).
- [84] Buchanan, R. C. *Ceramic Materials for Electronics*. Marcel Dekker, New York, 3rd edition, (1997).
- [85] Auciello, O., Scott, J. F., and Ramesh, R. *Phys. Today* **51**, 22 (1998).
- [86] Setter, N. *Electroceramic-Based MEMS*. Springer, New York, (2005).
- [87] Ahn, C. H., Rabe, K. M., and Triscone, J. M. *Science* **303**, 488 (2004).
- [88] Naumov, I. I., Bellaiche, L., and Fu, H. X. *Nature (London)* **432**, 737 (2004).
- [89] Dawber, M., Lichtensteiger, C., Cantoni, M., Veithen, M., Ghosez, P., Johnston, K., Rabe, K. M., and Triscone, J. M. *Phys. Rev. Lett.* **95**, 177601 (2005).
- [90] Lee, J. J., Thio, C. L., and Desu, S. B. *J. Appl. Phys.* **78**, 5073 (1995).

- [91] Ohtomo, A. and Hwang, H. Y. *Nature (London)* **427**, 423 (2004).
- [92] Cohen, R. E. *Nature (London)* **358**, 136 (1992).

Publications and Conferences

Peer-Reviewed Articles

- A. K. Tagantsev, G. Gerra, and N. Setter, *Phys. Rev. B* **77**, in press (2008).
- G. Gerra, A. K. Tagantsev, and N. Setter, *Phys. Rev. Lett.* **98**, 207601 (2007).
- A. K. Tagantsev and G. Gerra, *J. Appl. Phys.* **100**, 051607 (2006).
- G. Gerra, A. K. Tagantsev, N. Setter, and K. Parlinski, *Phys. Rev. Lett.* **96**, 107603 (2006).
- G. Gerra, A. K. Tagantsev, and N. Setter, *Phys. Rev. Lett.* **94**, 107602 (2005).

Conference Presentations

- G. Gerra, A. K. Tagantsev, and N. Setter, “Non-Electrostatic Size Effect in Ferroelectric-Electrode Thin Film Heterostructures”, *11th European Meeting on Ferroelectricity*, Bled, Slovenia, September 3–7, 2007.
- G. Gerra, A. K. Tagantsev, and N. Setter, “Size Effects in Ferroelectric Thin Films with Oxide Electrodes: a First-Principles Approach”, *International Conference on Nanoscience and Technology 2006*, Basel, Switzerland, July 30–August 4, 2006.
- G. Gerra, A. K. Tagantsev, N. Setter, and K. Parlinski, “Ionic Polarizability of Conductive Metal-Oxides and Critical Thickness for Ferroelectricity in BaTiO₃”, *2006 Workshop on the Fundamental Physics of Ferroelectrics*, Williamsburg, Virginia, USA, February 12–15, 2006.

Curriculum Vitae

GUIDO GERRA

Laboratoire de Céramique
École Polytechnique Fédérale de Lausanne
CH-1015 Lausanne
Switzerland

PERSONAL INFORMATION

- Date of birth: 21 October 1979
- Nationality: Italian

EDUCATION

- 2003: M.Phil. Materials Science (Honours), University of Cambridge, United Kingdom
- 2002: B.Sc. Physics (First Class Honours), University College London, United Kingdom
- 1998: Maturità Scientifica (50/60), Liceo Scientifico N. Copernico, Pavia, Italy
- 1997: High School Diploma (GPA: 3.93/4), Tempe High School, Tempe, AZ, USA

LANGUAGES

- English (fluent)
- Italian (native language)
- French (fluent)

AWARDS

- EPSRC Scholarship, University of Cambridge (2002–2003)
- Regent's Scholarship from Arizona State University for top 5% in class (1997)
- Top 10% in mathematics in the state of Arizona (1997)

PERSONAL INTERESTS

- Sports: soccer, swimming, running, skiing.
- Music: classical and electric guitar.
- Reading: science fiction, crime fiction, classic literature, history.